

Factors Influencing Roof-to-Ground Impact Severity: Video Analysis and Analytical Modeling

Nathan A. Rose
Gray Beauchamp
Stephen J. Fenton
Kineticorp, LLC

Copyright © 2007 SAE International

ABSTRACT

This paper explores the dynamics of rollover crashes and examines factors that influence the severity of the roof-to-ground impacts that occur during these crashes. The paper first reports analysis of 12 real-world rollover accidents that were captured on video. Roll rate time histories for the vehicles in these accidents are reported and the characteristics of these curves are analyzed. Next, the paper uses analytical modeling to explore the influence that the trip phase characteristics may have on the severity of roof-to-ground impacts that occur during the roll phase. Finally, the principle of impulse and momentum is used to derive an analytical impact model for examining the mechanics of a roof-to-ground impact. This modeling is used to identify the influence of various impact conditions on the severity of a roof-to-ground impact.

INTRODUCTION

This paper consists of two parts. Part I reports the results of video analysis carried out for 12 real-world rollover accidents. All twelve of these rollovers involved 1-½ rolls or more. Thus, statistically they fall within the top 15 percent of rollovers in terms of the number of quarter rolls. Nine of the twelve involved 2 rolls or more, placing them in the top 2.3% of rollovers in terms of the number of quarter rolls [1]. The purpose of the video analysis reported in this part was to examine the initial, peak and average roll rates that occurred during these multi-roll accidents and to identify points in the roll sequence where the vehicles experienced significant changes in roll velocity.

The research reported in this first part resulted in the following conclusions:

- The video analysis method used in this paper employed 90-degree roll angle intervals to generate roll rate time histories. Despite this relatively large sampling interval, this method will result in roll rate

time histories that generally lie within ± 50 degrees per second of the actual roll rate time history.

- The video analysis method employed in this paper results in considerable smoothing of the actual roll rate time histories. Thus, significant changes in roll velocity that occur over short durations in the actual roll rate time history occur over much longer durations in the roll rate time histories obtained with the video analysis method.
- For the twelve rollover accidents analyzed, the video analysis yielded initial roll rates between 150 and 540 degrees per second.
- The video analysis method yielded peak roll rates for these rollovers that varied between 300 and 675 degrees per second. These roll rates appeared highly dependent on the specific vehicle-to-ground impacts that were realized during the roll sequence.
- The video analysis method yielded peak roll rates during the times that the vehicles in these rollovers were on their roofs that varied between 300 and 600 degrees per second.
- The video analysis method yielded average roll velocities for these rollover accidents that varied between 144 degrees per second and 395 degrees per second.
- Vehicle-to-ground impacts that resulted in significant increases in roll velocity tended to occur early in the roll sequence whereas vehicle-to-ground impacts that resulted in significant decreases in roll velocity tended to occur later in the roll sequence. In all but one of the twelve cases, the first roll accelerated the roll velocity such that the peak roll velocity occurred downstream of the first roll.

Part II of this paper describes analytical models used to consider the trip phase of those rollover accidents that

begin with the vehicle being tripped and the roof-to-ground impacts that occur during the roll phase of a rollover accident. Results are reported from these models to identify factors that can contribute to the severity of a roof-to-ground impact. This part draws on the roll velocity time history characteristics identified in the first part to explore the levels of roof-to-ground impact severity that could be realized during a rollover accident.

When used in relationship to motor vehicle accidents, the term severity can have two distinct meanings. First, the term can refer to the exposure of the vehicle occupants to injury potential. For front, side, and rear impacts, a vehicle's center of mass (CoM) velocity change (ΔV) is commonly used with this meaning. Used in reference to occupant injury rates for front, side and rear impacts, the ΔV is an appropriate severity measure because the probability of occupant injury generally increases as the ΔV increases [2].

Alternatively, the term severity can refer to the demands placed on the vehicle structure by an impact. Used with this meaning, one severity measure for the vehicle structure would be the amount of energy that the vehicle structure is called on to absorb during the impact, with the severity increasing as the energy absorption demand on the vehicle structure increases. The ΔV experienced by a vehicle and the energy that that vehicle's structure is called on to absorb during an impact are related, but not equivalent, severity measures. For a given ΔV , the energy absorption demands placed on the vehicle structure depend on the stiffness of whatever that vehicle has impacted.

In this paper, the severity of a roof-to-ground impact is defined in terms of both ΔV and energy. ΔV s are calculated both at the vehicle CoM and at the roof-to-ground contact point. As far as the authors are aware, there are no studies in the technical literature that have attempted to correlate roof-to-ground impact ΔV s, either at the vehicle CoM or at the roof-to-ground contact point, to occupant injury rates. Rollovers have generally been treated with a more lumped parameter approach, with injury rates being correlated to parameters such as the number of rolls or pre-crash velocity [1, 3]. In our discussion here, no new statistical analysis of injury rates is presented and it is not our intent to propose an alternative metric for the overall severity of a rollover accident. However, based on the significance of the ΔV for front, side and rear impacts, it seems reasonable to expect that the likelihood that a belted, retained occupant will be injured during a *particular* roof-to-ground impact would increase as the CoM and ground contact point ΔV s increase.

The research reported in the second part of this paper resulted in the following conclusions:

- The characteristics of the trip force that initiates a rollover will, in part, determine the orientation and velocity conditions with which a vehicle enters the roll phase.
- The vehicle parameters will also be influential in determining the orientation and velocity conditions with which the vehicle enters the roll phase. In all of the scenarios considered in this paper, a passenger car configuration resulted in higher roll angles, roll velocities, and vertical velocities at the beginning of the roll phase than did a sport utility vehicle configuration.
- The vehicle orientation and velocity conditions that exist at the time the vehicle enters the roll phase are factors influencing the severity of the roof-to-ground impacts that will occur during the rollover. These conditions will most directly influence the severity of the first roof-to-ground impact.
- The severity of a roof-to-ground impact is determined by factors such as the vehicle's velocity conditions at impact, the orientation when the resultant collision force is transferred and the vehicle inertial properties.
- Severe roof-to-ground impacts are associated with either significant increases or significant decreases in roll velocity.
- Severe roof-to-ground impacts can occur during any portion of the roll sequence of a multi-roll accident. This statement is based on the observation that significant changes in roll velocity can occur throughout the roll sequence.
- The direction of force that results from a specific roof-to-ground impact will depend on the impact velocity conditions, the vehicle orientation at impact and the vehicle inertial properties. Roll velocity increases and roll velocity decreases will be associated with different force directions relative to the ground plane.

PART I – ANALYSIS OF ROLLOVER VIDEO

INTRODUCTION

Part I of this paper examines video footage of 12 real-world rollover accidents to develop an improved understanding of the roll rate time history characteristics of actual rollover events. This part contains two sections. The first section describes the methodology used for analyzing the video clips. The second section outlines and discusses the results obtained from the application of this video analysis methodology to the video footage of real-world rollovers. Roll rate curves were generated and reported for 11 of the 12 rollovers for which footage was analyzed. The video clips for this analysis were

collected from race footage, news clips, and police video. Using the video analysis method developed in the first section of this part, roll rate time histories were generated for the real-world accidents.

Once the roll rate time histories for the 12 cases were generated, the following questions were considered for each case:

- What was the magnitude of the peak roll velocity?
- When did this peak roll velocity occur?
- What was the average roll velocity?
- How many rolls occurred?
- Were there vehicle vaults that occurred during the roll sequence?
- Where did significant changes in roll velocity occur?
- What was the tripping mechanism?

VIDEO ANALYSIS METHOD

The video analysis method used in this paper consisted of counting the number of frames in the video over which the vehicles traversed each 90-degree interval of roll. Using a known frame rate, the number of frames for each 90-degree interval could be converted to time and the average roll velocity for each interval could be calculated. In this paper, this method will be referred to as the 90-degree interval method (90-DIM). The primary motivation for using 90-degree roll angle intervals had to do with the characteristics of the videos being used for the analysis. These videos were captured from perspectives that were not conducive to precise determinations of the vehicle roll angle. However, it was generally possible from these perspectives to determine when the vehicles in the videos completed each 90-degree interval of roll.

Such 90-degree intervals represented a relatively large sampling interval for plotting the roll rate time histories

for these rollovers. In fact, this sampling interval results in significant smoothing of the actual roll rate time histories. The overall accuracy of the 90-DIM and the magnitude of the smoothing effect introduced by this method were quantified in two ways.

First, roll rate sensor data was examined from NHTSA Test #2553, a 30 mph dolly rollover test run by the Transportation Research Center on February 28, 1997. The test report and sensor data for this test can be accessed via NHTSA's research and development website (<http://www-nrd.nhtsa.dot.gov>). Figure 1 depicts the roll dynamics for this test using a number of frames from the test video.

To determine the effect of the 90-degree sampling intervals used in this paper, the roll rate sensor data for this test was analyzed to generate a roll angle time history. The raw roll rate sensor data had a sampling rate of 8000 Hz. Before generating the roll angle time history, this data was sampled down to 1000 Hz for ease of analysis. The roll angle time history generated from this 1000 Hz data was then sampled to 33 Hz to bring it down into the range of samples (frames) available in the videos used for this paper (around 30 frames per second). Finally, this roll angle data was sampled with 90-degree roll angle intervals and these data points were used to generate a new roll rate time history. This roll rate time history generated with 90-degree roll angle intervals was plotted against the original, actual roll rate time history.

Figure 2 depicts the actual roll rate time history and the roll rate time history generated with 90-DIM. The squares along the 90-DIM curve denote the average velocities for each 90-degree interval, plotted at the interval midpoints. The dark line connecting these points is a curved line generated by Microsoft Excel using cubic spline interpolation [4].

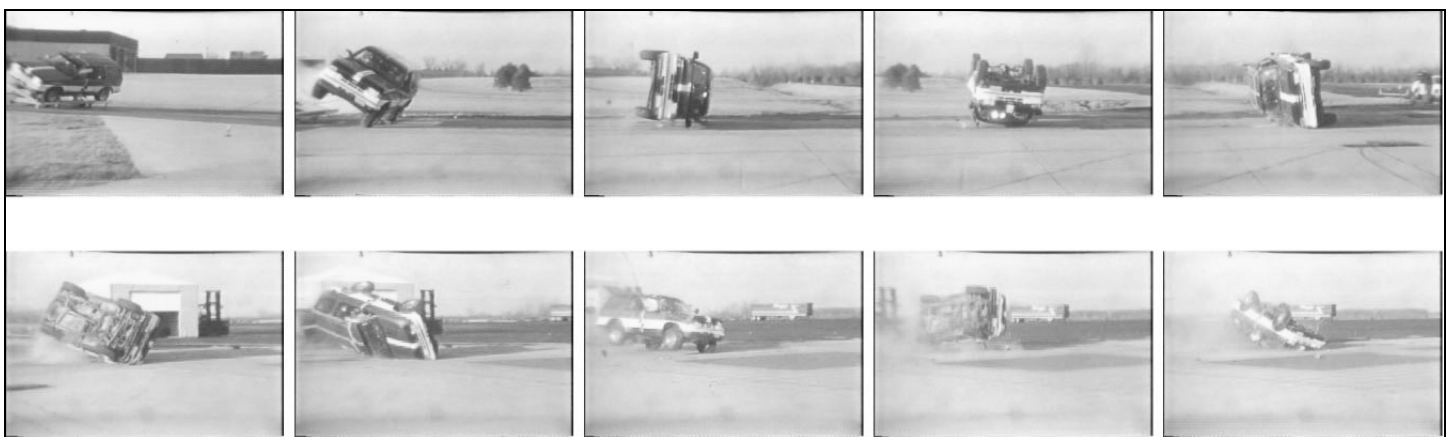


Figure 1 – Roll Dynamics for NHTSA Test #2553

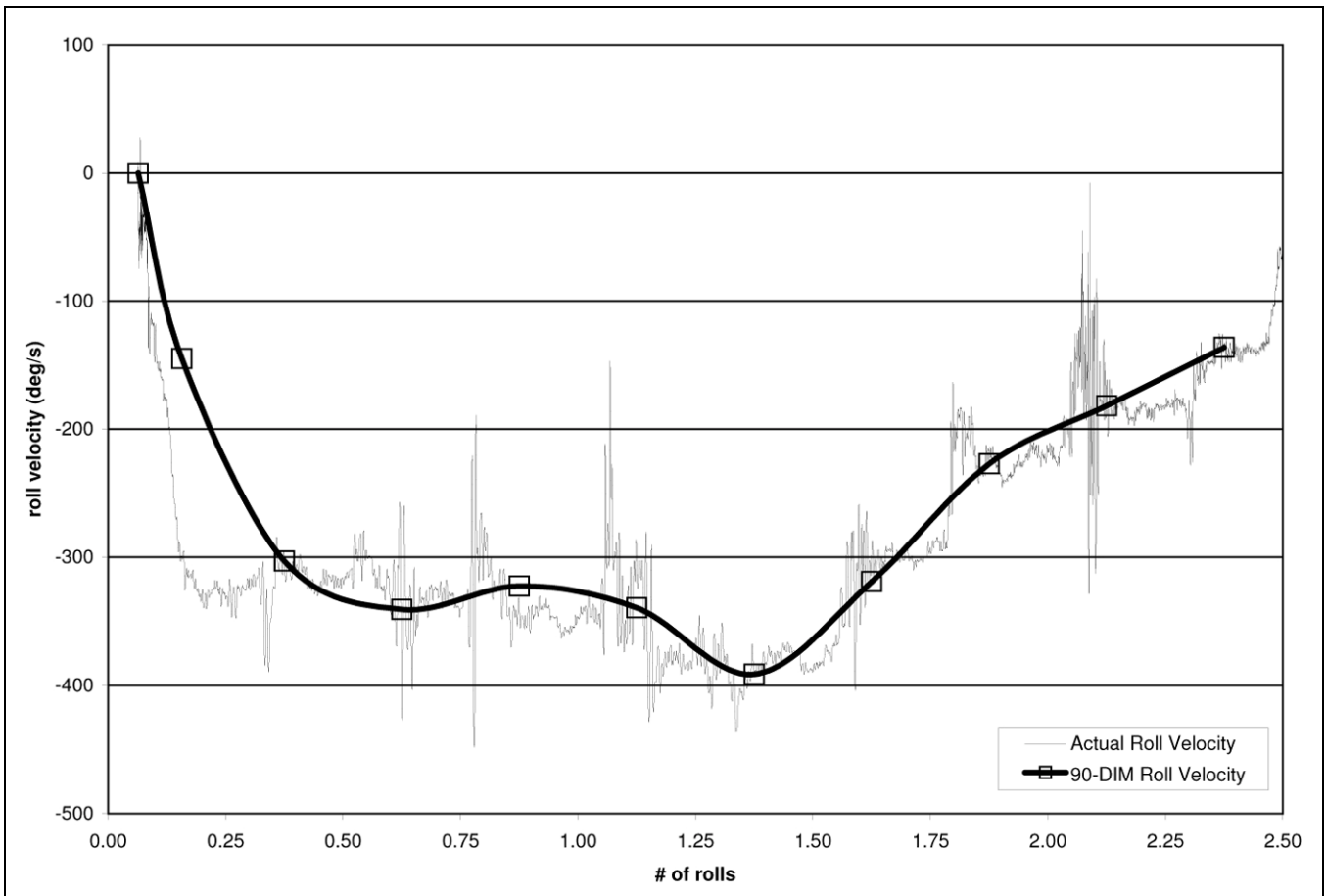


Figure 2 – Roll Rate Time Histories for NHTSA Test #2553

A number of observations can be made from examining Figure 2. First, after the first ¼ roll, the 90-DIM produced a roll velocity time history that generally captured the actual roll velocity time history. On the other hand, the 90-DIM resulted in considerable smoothing of the actual roll velocity data. Substantial changes in roll velocity that occurred quickly in the actual roll velocity data occurred much more slowly in the roll velocity curve generated with 90-degree roll angle intervals. For instance, in the actual roll velocity data, there was a change in roll velocity of approximately 100 degrees per second that occurred over a time period of approximately 30 milliseconds in the area of 1-¾ rolls. This same change in velocity occurred between 1.7 and 2 rolls in the 90-DIM curve, a period of approximately 250 milliseconds. In addition to the smoothing, the curve generated with the 90-DIM did a relatively poor job of capturing the build up of roll velocity that occurred during the first ¼ roll. The reason for this is that this first 90-degree interval contains the trip phase of this rollover, during which large changes in roll velocity are occurring.

The effects of the 90-degree sampling intervals were also examined using six rollover simulations generated with PC-Crash [5]. Using PC-Crash allowed for the use of camera views and video frame rates that were similar to those present in the real world videos analyzed later. These simulations were run with varying initial conditions and vehicle parameters. The first five simulations

involved roll rates below 500 degrees per second. In the last simulation the roll rate exceeded 500 degrees per second. Each animation was imported into Adobe Premier for frame-by-frame analysis and the number of frames corresponding to each 90-degree interval of vehicle roll was recorded. Since each of these animations contained 30 frames per second, the duration of each 90-degree interval could be calculated using the following formula:

$$\Delta t_{90} = \frac{\eta_{90}}{30} \quad (1)$$

In Equation (1), Δt_{90} is the interval duration and η_{90} is the number of frames. Once the duration of each interval was known, the average roll velocity during each interval was calculated using the following formula:

$$\omega_{r, avg} = \frac{\Delta \theta}{\Delta t_{90}} \quad (2)$$

In Equation (2), $\Delta \theta$ is the change in roll angle of the vehicle, 90 degrees in this case, and $\omega_{r, avg}$ is the average roll velocity for the interval. For each of the PC-Crash simulations, the average roll velocities generated with video analysis and with Equation (2) were plotted versus the number of rolls.

In order to assess the ability of these roll velocity time histories to characterize the actual instantaneous roll velocity curves, roll velocity data was exported from each PC-Crash simulation and this data was plotted against the roll velocity curves obtained from the video analysis. Figure 3 contains roll velocity time histories for the first PC-Crash simulation, which will be referred to as Case A. The squares along the 90-DIM roll velocity curve denote the average velocities for each 90-degree interval, plotted at the interval midpoints. The thick line connecting these squares is a curved line generated by Microsoft Excel using cubic spline interpolation [4]. The thin line is the actual roll velocity time history. Appendix A contains similar roll velocity plots for Cases B through E.

As these figures show, the roll velocity time history generated with the 90-DIM provided a reasonable approximation of the actual roll velocity curve. In each of these five cases, the actual instantaneous roll rate curve was generally contained within a roll velocity envelope lying within ± 50 degrees per second of the average roll velocity curve from the video analysis. As with the previous analysis of the dolly rollover, one important difference between the roll velocity time histories generated with the 90-DIM and the actual roll velocity time histories from the simulations was that changes in roll velocity occurred over a much longer time period for the video analysis curve than they did for the actual curve. As will be discussed in Part II, the time period

over which a change in roll velocity curve occurs affects the severity of a vehicle-to-ground impact. Specifically, severe roof-to-ground impacts will be associated with quick, significant changes in roll velocity.

Also similar to the previous analysis of the dolly rollover, the 90-DIM did not adequately capture the build-up of roll velocity during the first $\frac{1}{4}$ roll. This is not surprising and is due to the fact that the entire trip phase is contained within the 0 to 90 degree roll angle interval. In order to obtain a meaningful initial roll rate, the authors did not include the first 45 degrees of roll in the analysis. Thus, the first roll angle interval was reduced to 45 degrees. When this modification was made in the PC-Crash cases, the initial roll rate was found to fall within the ± 50 degree per second envelope discussed previously. This technique was used in our analysis of the initial roll rates for the real-world cases.

For the sixth PC-Crash case, Case F, a ± 50 degree per second envelope was found to be insufficient to bound the actual roll velocity time history when 90-degree roll angle intervals were used. This increase in the potential error occurred because of the high the roll rate that was achieved in this simulation. This simulation had a peak roll velocity of 650 deg/sec and roll velocities of nearly 500 degrees per second were sustained for the first 2 seconds of the sequence. At such high roll rates, the roll angle of the vehicle changed substantially between each frame of video.

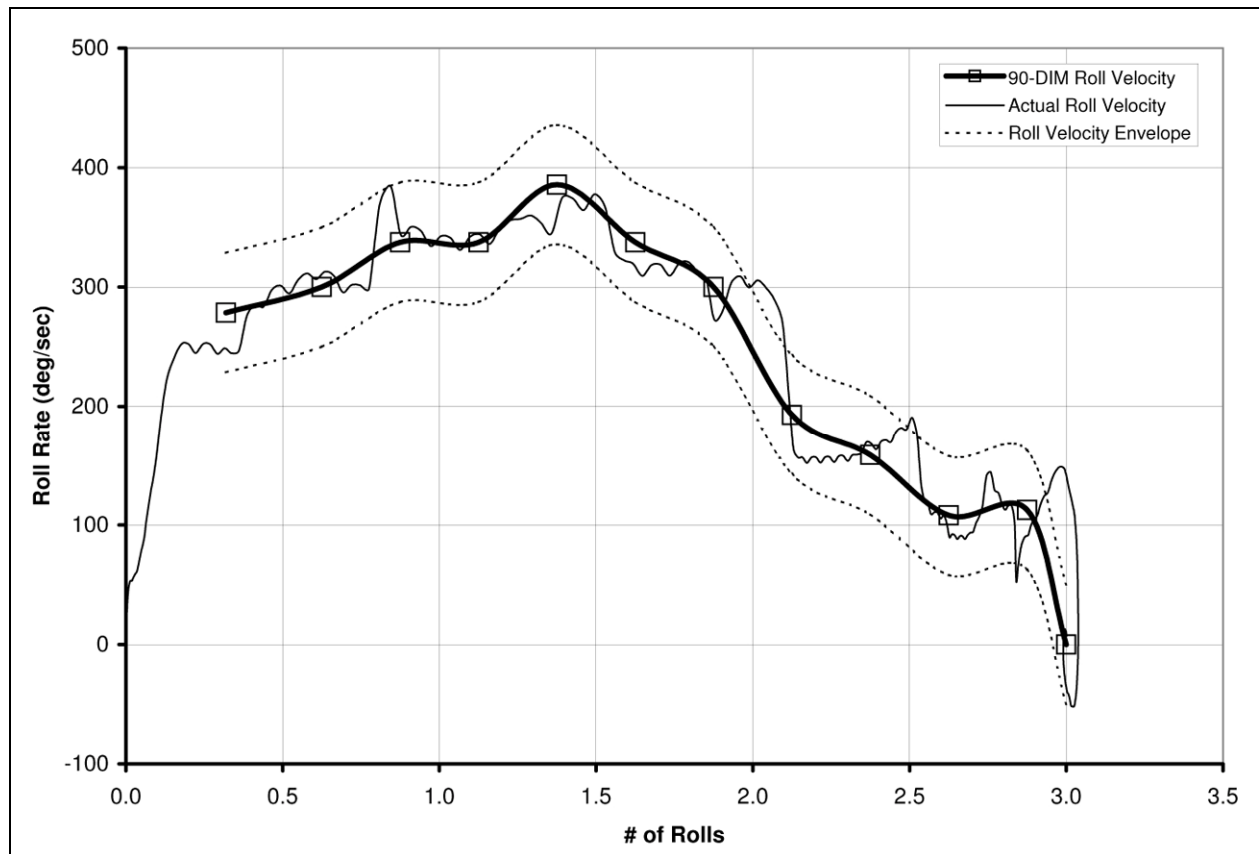


Figure 3 – Roll Rate v. Number of Rolls, PC-Crash Case A

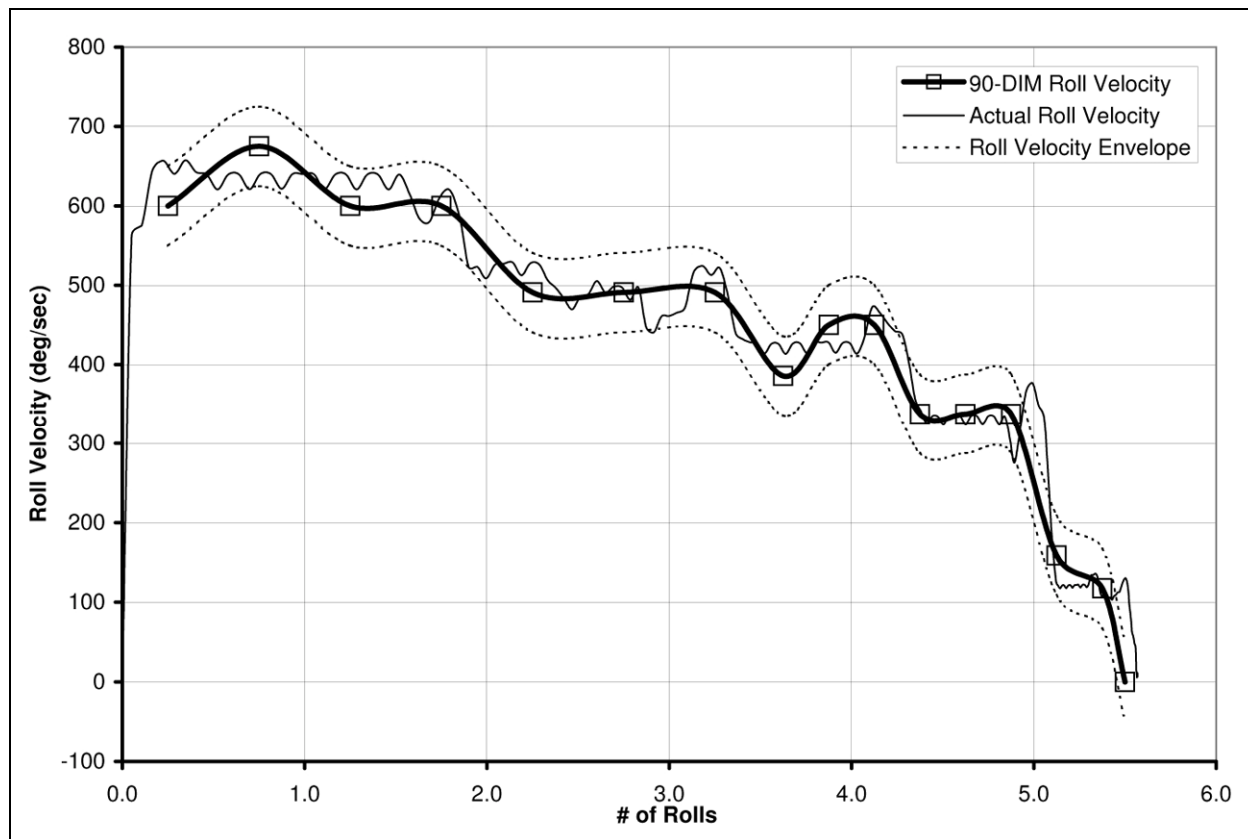


Figure 4 – Roll Rate v. Number of Rolls, PC-Crash Case F

This case was reanalyzed with a modified technique. When the roll rate exceeded 450 degrees per second, the analyst switched to counting frames over 180-degree intervals instead of 90-degree intervals. Figure 4 contains roll velocity curves for this case generated with this modified method. By applying this modification, the actual curve became contained within a ± 50 degree per second roll rate envelope and the general shape of the video analysis roll rate time history more closely resembled the actual curve. The real-world cases that exhibited high roll rates were analyzed using this same tactic.

ANALYSIS OF REAL-WORLD ROLLOVER EVENTS

This section describes the results of analyzing video clips of twelve real-world rollovers using the previously described modified 90-DIM. Table 1 is a summary of the results from the twelve cases that were analyzed. For each case, this table lists the vehicle type, trip type, number of rolls, and the initial, peak and average roll rates. In addition to Table 1, this section also includes discussion of each individual case.

These clips were collected from rally car race footage, news footage, and police footage. Both video analysis curves and roll rate envelopes were determined for each real-world case. Prior to this analysis, each video was analyzed in an attempt to determine whether the video was playing at real time or not. Several features of the

video were examined to conduct this analysis. Audio was included in many of the clips and was a good indicator that speed alteration had not occurred. Even small alterations in audio speed, produce an identifiable sound signature. Visual clues were also used to determine if a clip's speed had been altered. Smoke, dust and people running are some of these visual clues.

All of the video clips had a timebase of 30 frames per second. However, in some of the rally car footage, every 5th frame was repeated. This is likely due to the fact that many rally racing events take place in Europe and are captured using PAL format rather than NTSC which is standard in the United States. In the context of this study, the major difference between the two formats are that PAL format videos contain 25 frames per second and NTSC format videos contain 30. Thus, when a PAL video clip is edited in the NTSC format, the software repeats every 5 frames to avoid altering the speed of the video segment. For this paper, two different approaches were used to analyze the video clips that contained repeated frames. First, the repeated clips were deleted and the average roll rates were calculated assuming 25 frames per second. Second, the authors used Adobe Premier to determine which of the two consecutive frames was the actual frame and which was the repeated frame. The clip was then analyzed at 30 frames per second. The results between these two methods were in agreement.

Case #	Vehicle Type	Trip Type	# of Rolls	Initial Roll Rate (deg/sec)	Peak Roll Rate (deg/sec)	Peak Roll Rate on Roof (deg/sec)	Average Roll Rate (deg/sec)
1	pickup truck	off road furrow	2	245	386	300	247
2	large SUV	on road	1.75	270	415	300	338
3	large SUV	off road furrow	3.75	208	450	450	302
4	rally car	impact	4	540	573	500	272
5	road race	off road furrow	2.25	338	338	338	173
6	rally car	impact	3	169	476	476	261
7	rally car	ramping	5	169	491	491	310
8	rally car	drop off road	4	225	386	386	174
9	rally car	impact	1.5	270	300	300	190
10	rally car	impact	1.5	225	338	300	144
11	rally car	dirt road furrow	7	150	675	600	395
12	rally car	off road furrow	4	-	-	-	-

Table 1 – Results from the Real-World Cases

In addition to these timebase issues, the quality of the real-world video varied from case-to-case. However, the cases presented in this section were selected based on the authors' ability to identify 90-degree roll angle intervals. The quality of each of these cases was found to be adequate for analysis reported in this section.

Case #1: The roll sequence and roll curve for Case 1 are depicted in Figures 5 and 6. Case 1 is a rollover that was captured on video from the front of a police cruiser. A pickup truck going around a left hand curve traveled into the right shoulder. The driver steered the vehicle back onto the roadway, and then, back to the right. The truck spun out and exited the right side of the road in a clockwise yaw, entered a field, and began rolling. The truck rolled past two rolls by about 45 degrees and then rocked back onto its tires. In this case, the vehicle's roll velocity increased early in the roll sequence and peaked after approximately 1 roll. Between 1- $\frac{1}{4}$ and 1- $\frac{3}{4}$ rolls the vehicle experienced a change in roll velocity on the order of 125 degrees per second. This change in roll velocity likely occurred over a shorter duration than that indicated by the video analysis roll rate time history of Figure 6.

Case #2: The roll sequence and roll curve for Case 2 are depicted in Figures 7 and 8. Case 2 involved a large SUV in a police chase and the video was taken from a helicopter. The SUV attempted to pass another vehicle on the on-ramp of an interstate. The SUV clipped the other vehicle, steered to the left, traveled over the end section of a short curb, and entered the interstate in a counter-clockwise yaw. The vehicle then tripped and began rolling across the interstate. After rolling 1- $\frac{1}{4}$ times, the SUV impacted the concrete median barrier. The impact vaulted the SUV over the barrier, where it came to rest in oncoming lanes of traffic after rolling a total of 1- $\frac{3}{4}$ times.

The SUV deposited tire marks and gouge marks on the roadway prior to rolling. The leading front wheel began gouging the pavement shortly after contacting the curb

and this wheel deposited a gouge for approximately 50 feet prior to the beginning of the roll phase. The rear wheel gouged for only a short distance prior to trip. Once the vehicle began to roll, markings on the pavement were visible after each ground impact. In this case, the leading roof rail (passenger's side) contacted the ground first. The driver's side roof was the next to contact the ground. The vehicle was then vaulted into the air as result of the passenger side tires impacting the ground. The vehicle was still airborne when it impacted the barrier.

Case #3: The roll sequence and roll curve for Case 3 are depicted in Figures 9 and 10. Case 3 also involved an SUV in a police chase with the video being captured from a helicopter. Initially, the SUV was traveling down a freeway. Prior to reaching a bridge that passed over another freeway, the SUV traveled into the right grass shoulder. The SUV hit a grass embankment and became airborne, clearing the freeway below. Upon landing on the grass shoulder, the SUV entered a counter-clockwise yaw and then rolled 3- $\frac{3}{4}$ times. It appears in the video that the airborne phase significantly contributed to tripping the vehicle.

In this case, the vehicle experienced an increase in roll velocity of approximately 250 deg/sec during the second $\frac{1}{2}$ roll. The roll velocity then remained above 400 deg/sec until the vehicle reached approximately 2- $\frac{3}{4}$ rolls. Between 2- $\frac{3}{4}$ and 3- $\frac{1}{4}$ rolls, the vehicle experienced a large decrease in roll velocity of approximately 175 deg/sec.

Case #4: The roll sequence and roll curve for Case 4 are depicted in Figures 11 and 12. A vehicle in a rally race exited the left edge of the roadway in a clockwise yaw. The vehicle then impacted a ditch that ran perpendicular to the roadway and tripped with its driver's side leading. This ditch impact vaulted the vehicle into the air where it completed 2- $\frac{3}{4}$ rolls before returning to the ground. The vehicle went on to roll an additional 1- $\frac{1}{4}$ times (4 total rolls) and came to rest on its wheels.

This rollover had the highest initial roll rate of all cases. This can be attributed to the unique engagement with the ditch that tripped the vehicle. The roll initiation was similar to a curb trip except that, along with the tires, the rocker panel also engaged the ditch. The rocker panel was able to absorb higher forces than the tires would have absorbed alone. This resulted in a high initial roll rate and a high vault height. When the vehicle impacted the ground for the first time, the roll rate was reduced from approximately 570 deg/sec to 338 deg/sec.

Case #5: The roll sequence and roll curve for Case 5 are depicted in Figures 13 and 14. A sports car in a road race exited a right hand curve in a clockwise yaw then steered to the left and entered a counter-clockwise yaw. The rear tires of the vehicle entered the right side grass shoulder and the vehicle began to roll. It appeared that uneven terrain off the side of road contributed to the tripping of the vehicle. The roll itself took place on the asphalt surface and the vehicle ultimately rolled 2-¼ times. The vehicle stalled at 2-¼ rolls for several seconds and then rolled back onto its tires.

An interesting feature of this accident is the vaulting, both at trip, and during subsequent points in the roll. The initial vault rotated the vehicle enough so that the entire roof missed the ground during the first roll. The first ground impact was to the driver's side of the vehicle. The vehicle then continued to rotate until the driver's side tires impacted ground, vaulting the vehicle several feet into the air. The next ground contact was a major impact to the passenger side. When the driver's tires impacted the ground a second time, the vehicle was once again vaulted into the air.

Case #6: The roll sequence and roll curve for Case 6 are depicted in Figures 15 and 16. Case 6 occurred on a dirt track with grassy shoulders. While traveling through a left hand turn, the vehicle left the right side of the road in a counter-clockwise yaw and impacted a bank that ran parallel to the road. The impact with the bank reversed the yaw direction, vaulted the vehicle into the air and induced roll. After the bank impact, the vehicle landed on its driver's side rolling a total of 3 times through the shoulder. In this case, the vehicle's roll velocity increased significantly during the first half roll and decreased significantly at around 2 rolls and 2-½ rolls.

Case #7: The roll sequence and roll curve for Case 7 are depicted in Figures 17 and 18. This rollover occurred in an S-curve section of a race. The vehicle traveled straight through the first part of the turn impacting a bank. The left side of the vehicle ramped up the embankment causing the vehicle to roll onto its roof in a corkscrew-like manner and to yaw counter-clockwise. The vehicle eventually rolled a total of 5 times down the dirt roadway. The roll rate remained low in this accident until the roll motion transition from a corkscrew-type motion to a barrel roll, after approximately 1 roll. When

the tires touched down for the first time, the vehicle vaulted into the air and the roll rate was accelerated. The peak roll rate occurred at approximately 1-¾ rolls.

Case #8: The roll sequence and roll curve for Case 8 are depicted in Figures 19 and 20. The rally car went off the right side of the track while traversing a left hand turn. At the edge of the road was a steep drop-off to a grassy field that sloped downhill. The vehicle went over the drop-off passenger side leading and the passenger side of the vehicle began to fall. The vehicle impacted the field below at a roll angle of approximately 45 degrees. The vehicle then rolled 4 times through the grassy field..

Case #9: The roll sequence and roll curve for Case 9 are depicted in Figures 21 and 22. The vehicle in this case traversed a left hand corner too wide, traveled off the right side of the road and impacted an embankment. The impact caused the vehicle to yaw clockwise, vault into the air and roll driver's side leading. The impact also pitched the vehicle so that the first area to contact the ground was the rear passenger side of the roof. This impact to the rear of the roof caused the vehicle to football and impact the front tires as it completed one roll. The vehicle went on to traverse an additional ½ roll and came to rest on its roof.

Case #10: The roll sequence and roll curve for Case 10 are depicted in Figures 23 and 24. Case 10 involved a small hatchback vehicle in a race. The vehicle exited the right side of the dirt track in a counterclockwise yaw while traversing a left hand corner. The vehicle then impacted the ditch on the right side of the road which reversed the yaw direction and tripped the vehicle. The vehicle then rolled 1-½ times down the dirt track.

Case #11: The roll sequence and roll curve for Case 11 are depicted in Figures 25 and 26. The vehicle came over a hill at a high rate of speed and became airborne. Upon landing, the vehicle lost control and began rolling down the dirt track, driver's side leading. The roll rate in this case started out the lowest of any case and peaked out higher than any case. This appeared to be directly related to the high speed at which the vehicle was traveling when it tripped. The vehicle in this case rolled 7 times, more than any other case study.

Case #12: The roll sequence for Case 12 is depicted in Figures 27. The vehicle in this case exited the right side of the dirt track in a counter-clockwise yaw. The rear wheels of the vehicle left the dirt road first and began furrowing in the softer soil eventually tripping the vehicle. The vehicle rolled 4 times through the grass shoulder. The choppy video could not be analyzed to determine roll rates. However, some interesting vaulting was noted. Although the vehicle rolled a total of 4 times, it appears the roof only contacted the ground during the fourth roll. The vehicle is clearly airborne due to vault between approximately 1-¼ and 1-¾ rolls and again between 2-¼ and 2-¾ rolls.



Figure 5 – Roll Sequence, Real-World Case #1

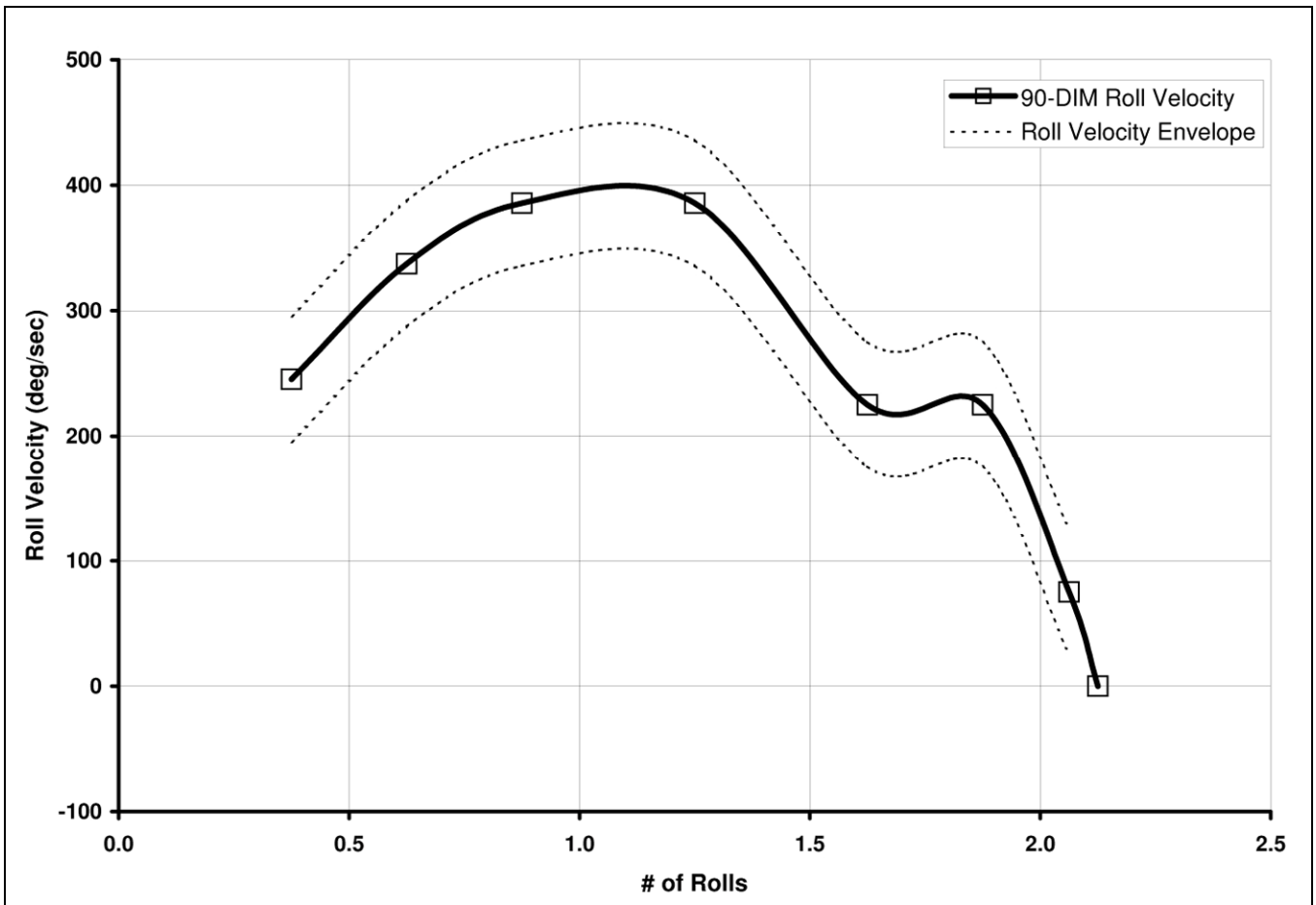


Figure 6 – Roll Velocity v. # of Rolls, Real-World Case #1



Figure 7 – Roll Sequence, Real-World Case #2

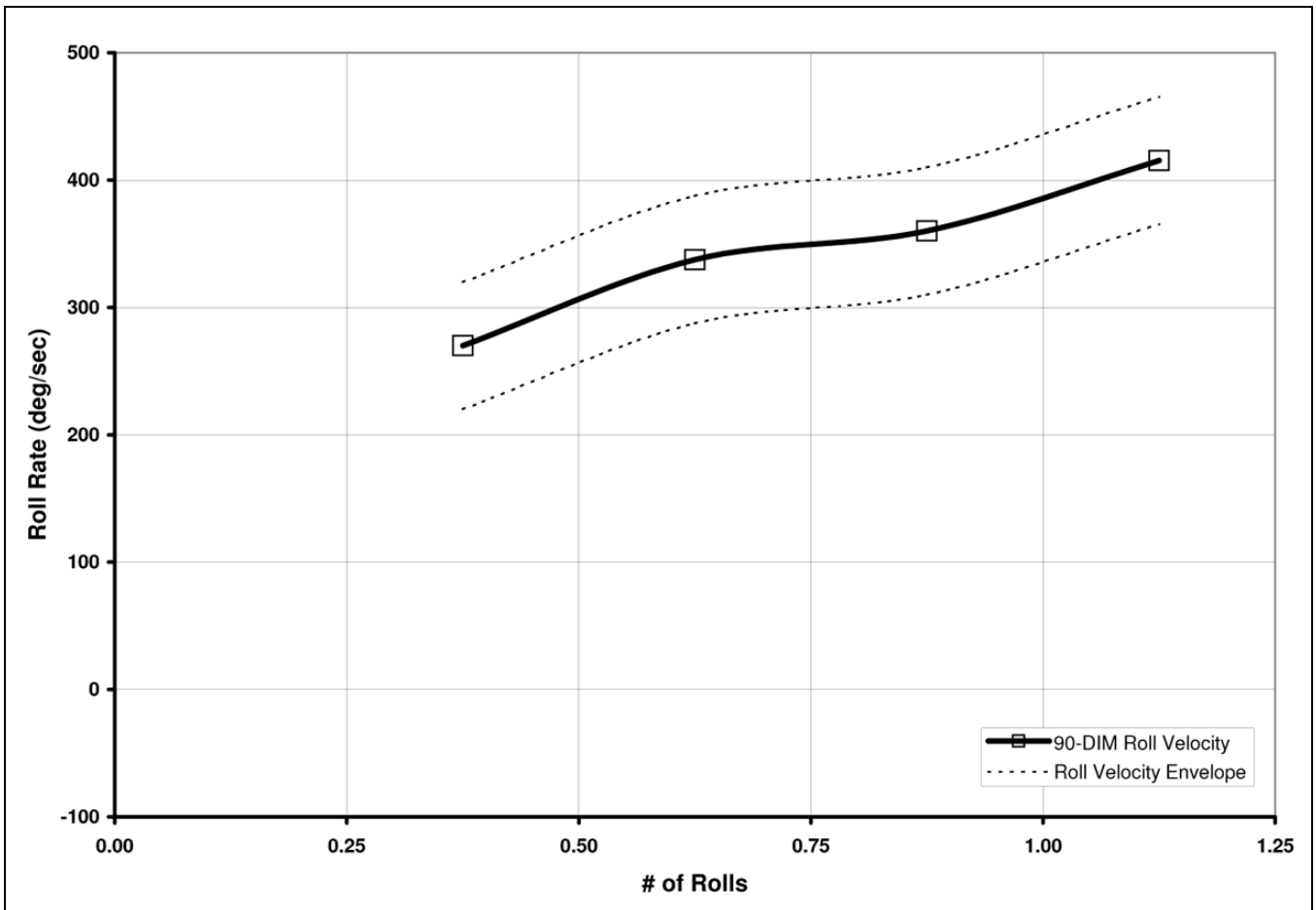


Figure 8 – Roll Velocity v. # of Rolls, Real-World Case #2



Figure 9 – Roll Sequence, Real-World Case #3

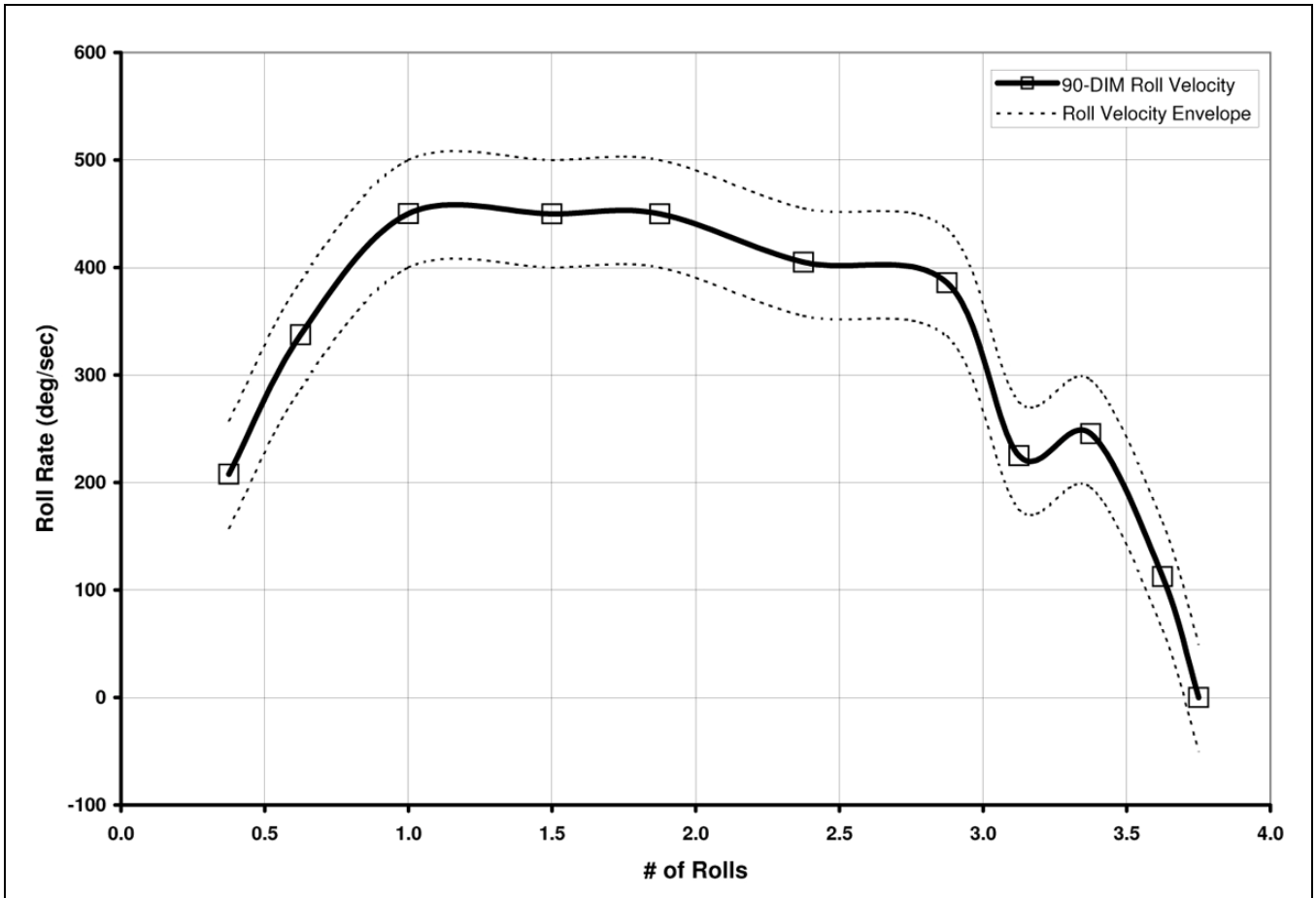


Figure 10 – Roll Velocity v. # of Rolls, Real-World Case #3



Figure 11 – Roll Sequence, Real-World Case #4

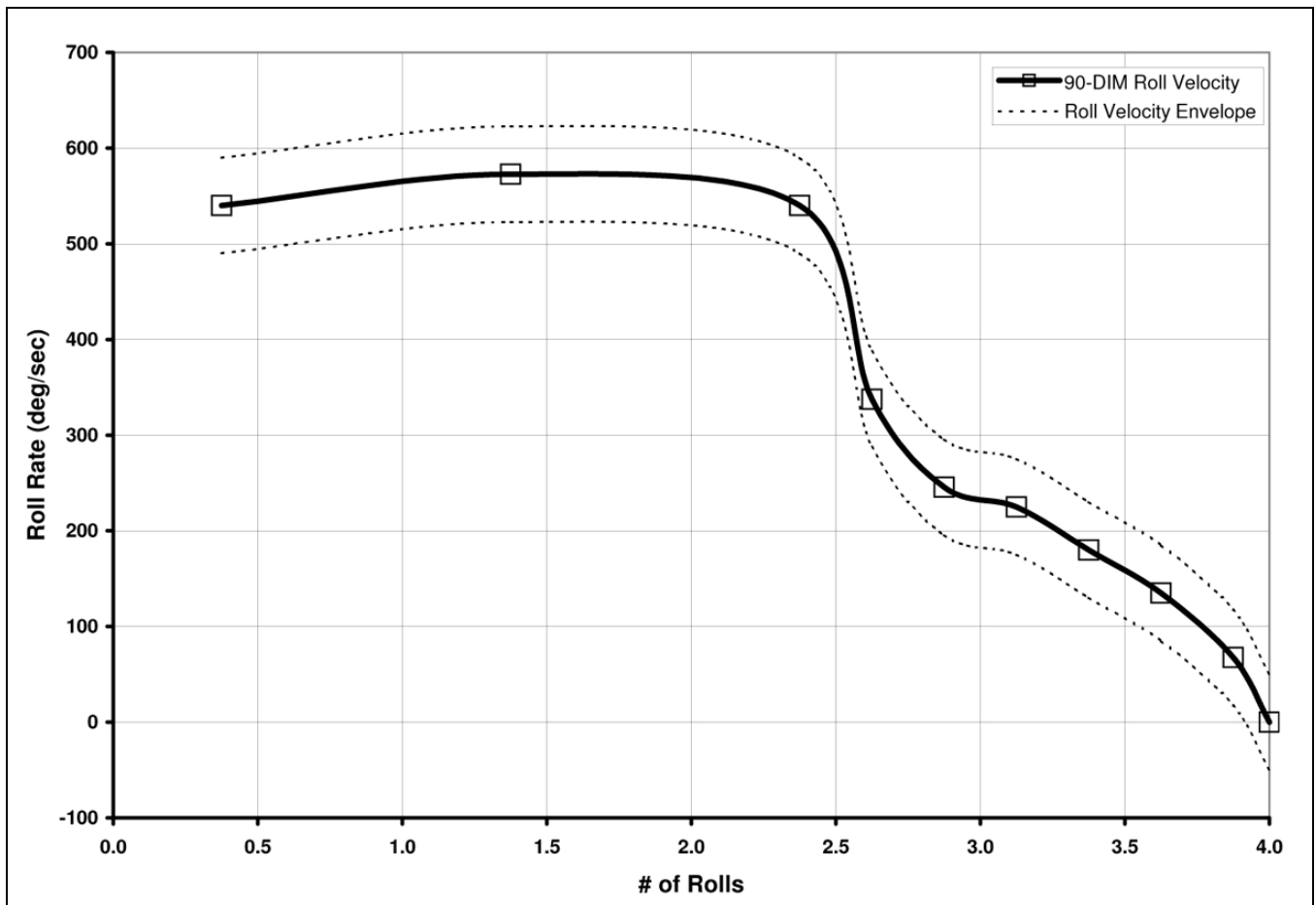


Figure 12 – Roll Velocity v. # of Rolls, Real-World Case #4



Figure 13 – Roll Sequence, Real-World Case #5

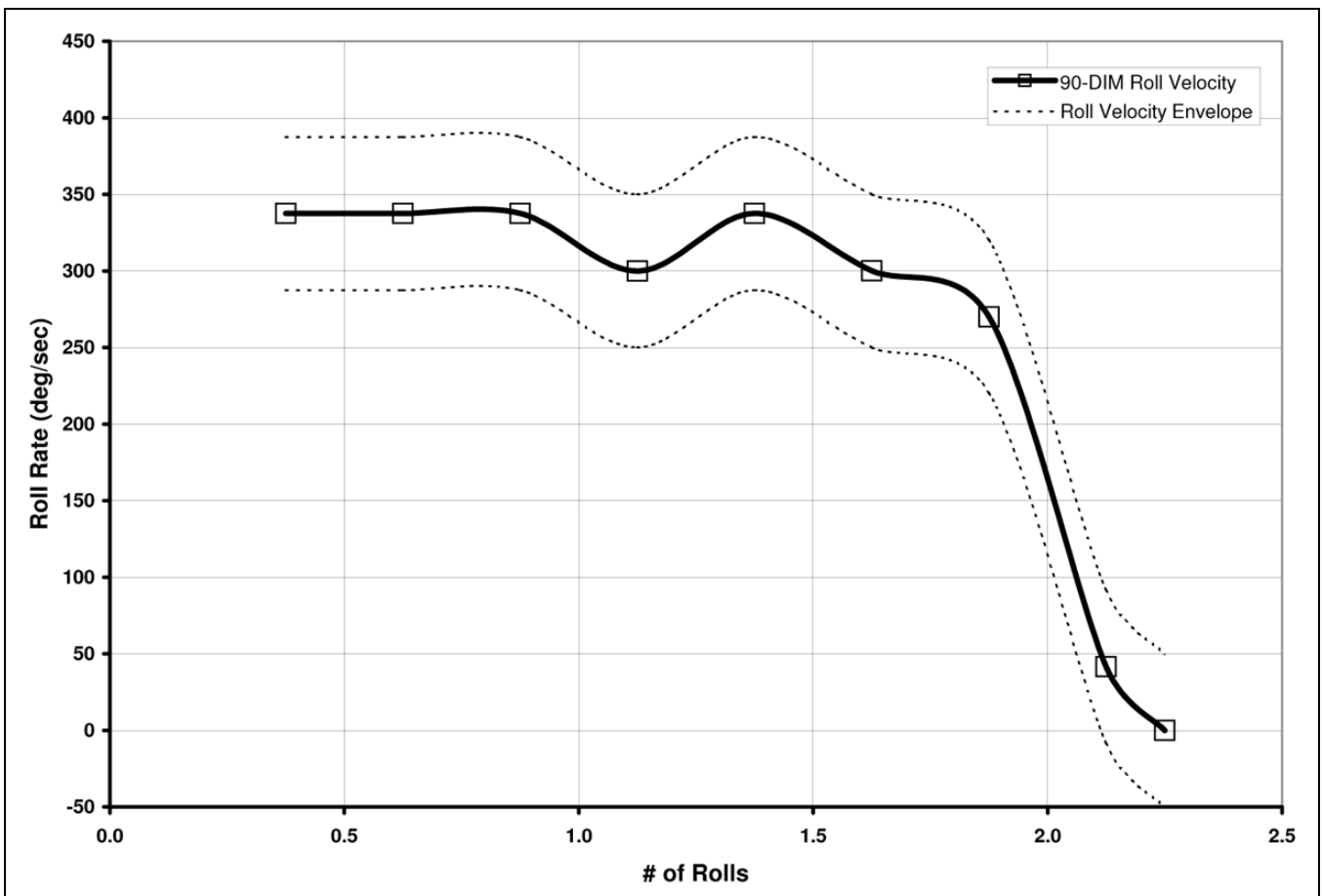


Figure 14 – Roll Velocity v. # of Rolls, Real-World Case #5



Figure 15 – Roll Sequence, Real-World Case #6

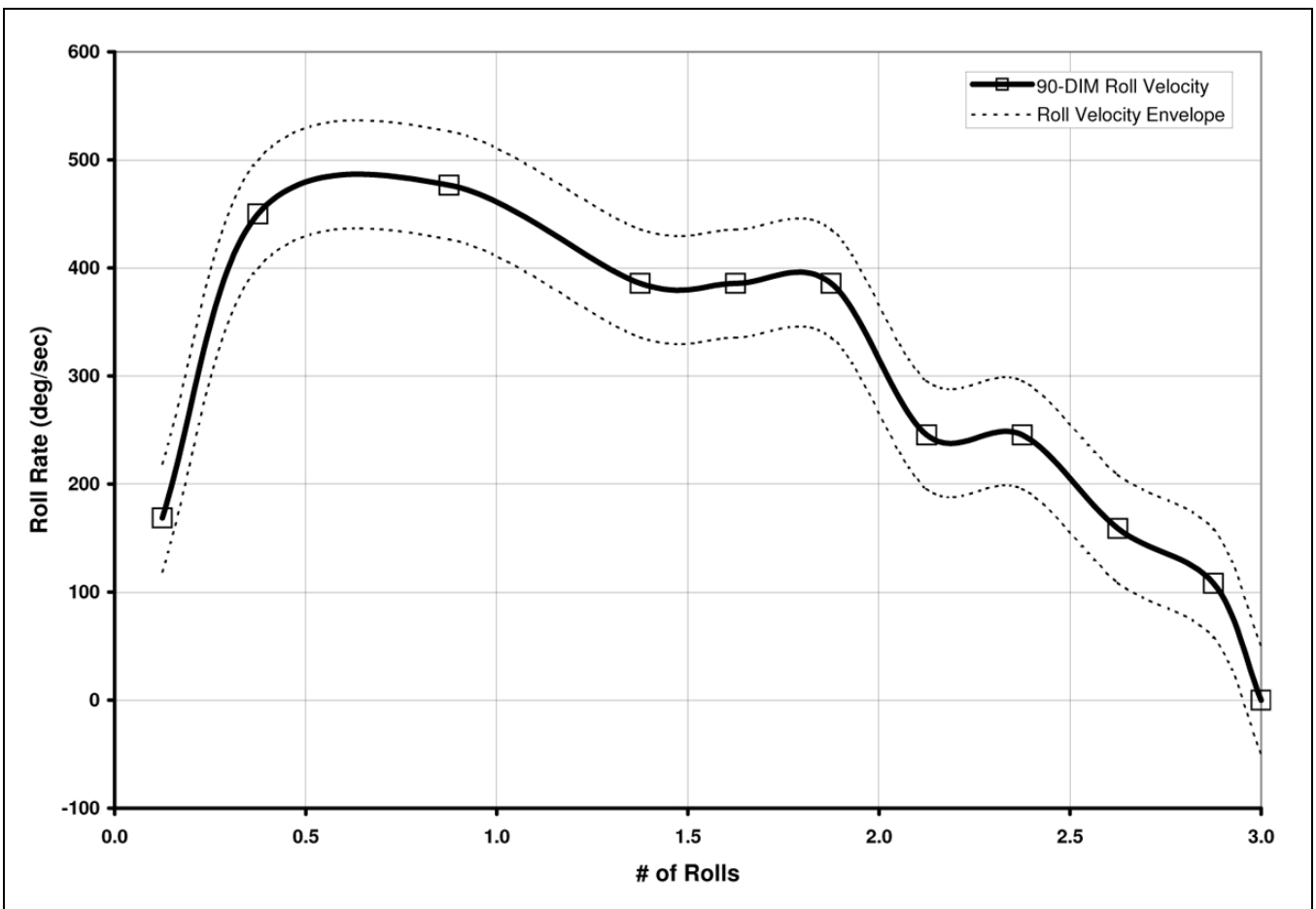


Figure 16 – Roll Velocity v. # of Rolls, Real-World Case #6



Figure 17 – Roll Sequence, Real-World Case #7

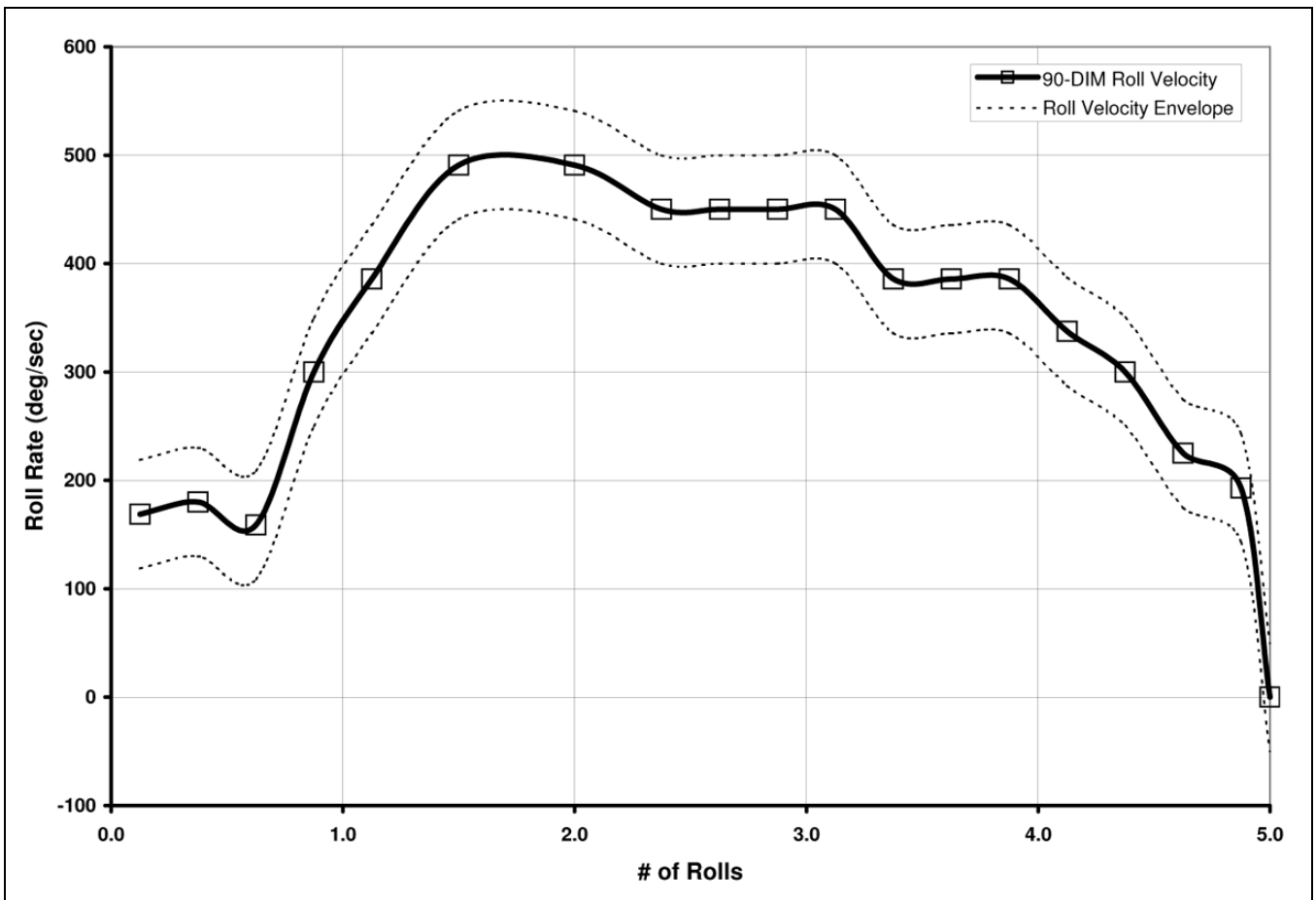


Figure 18 – Roll Velocity v. # of Rolls, Real-World Case #7



Figure 19 – Roll Sequence, Real-World Case #8

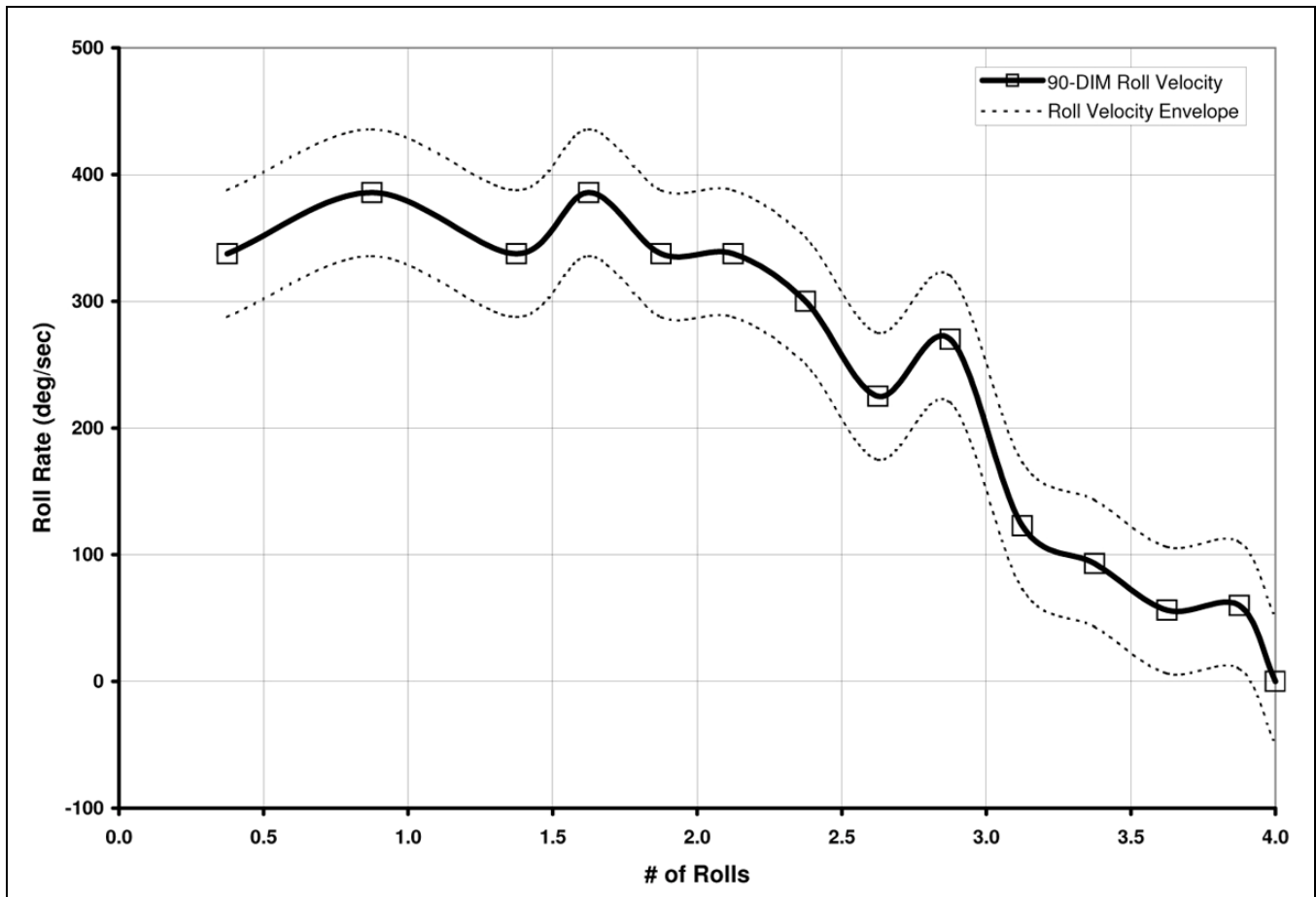


Figure 20 – Roll Velocity v. # of Rolls, Real-World Case #8



Figure 21 – Roll Sequence, Real-World Case #9

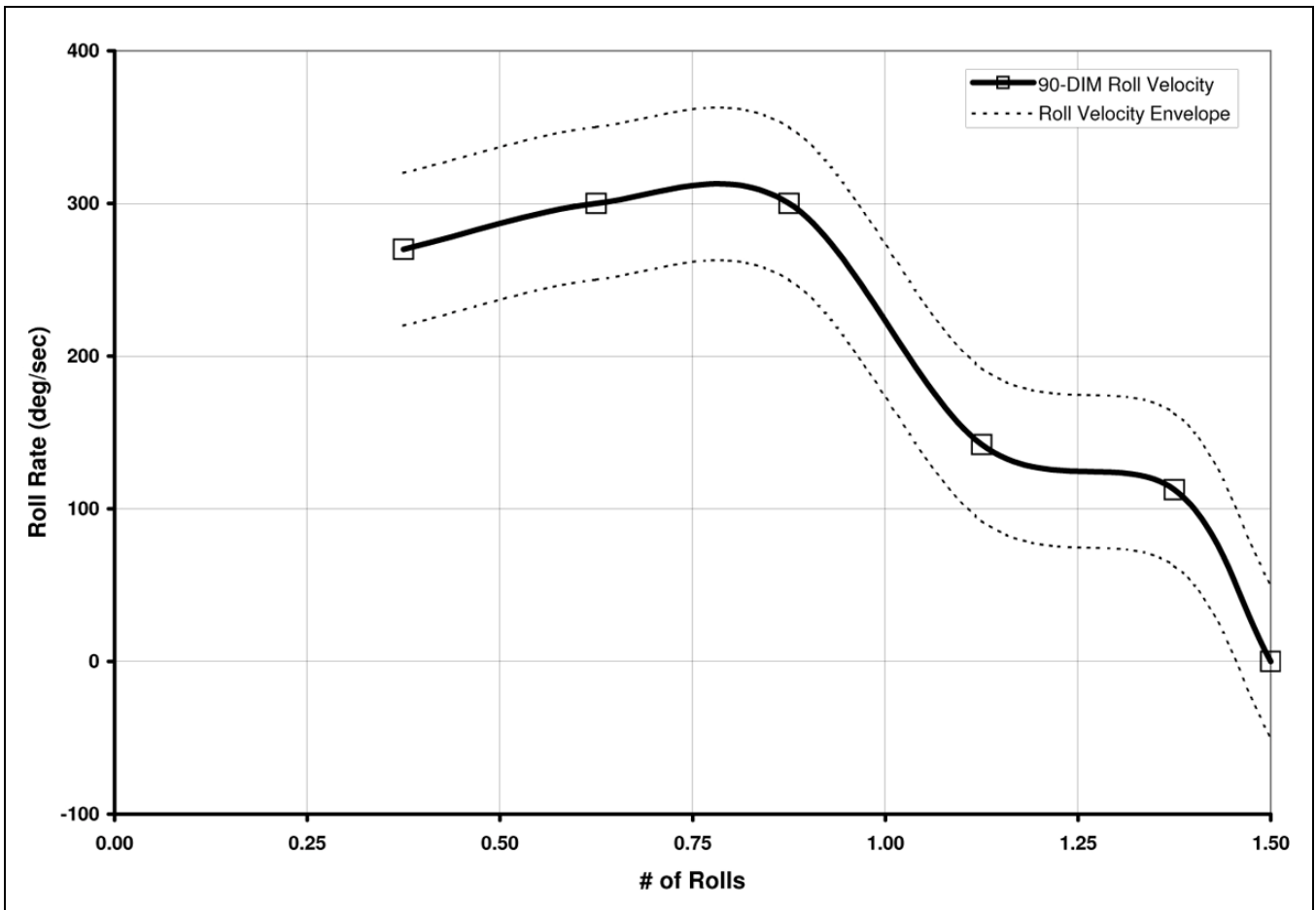


Figure 22 – Roll Velocity v. # of Rolls, Real-World Case #9



Figure 23 – Roll Sequence, Real-World Case #10

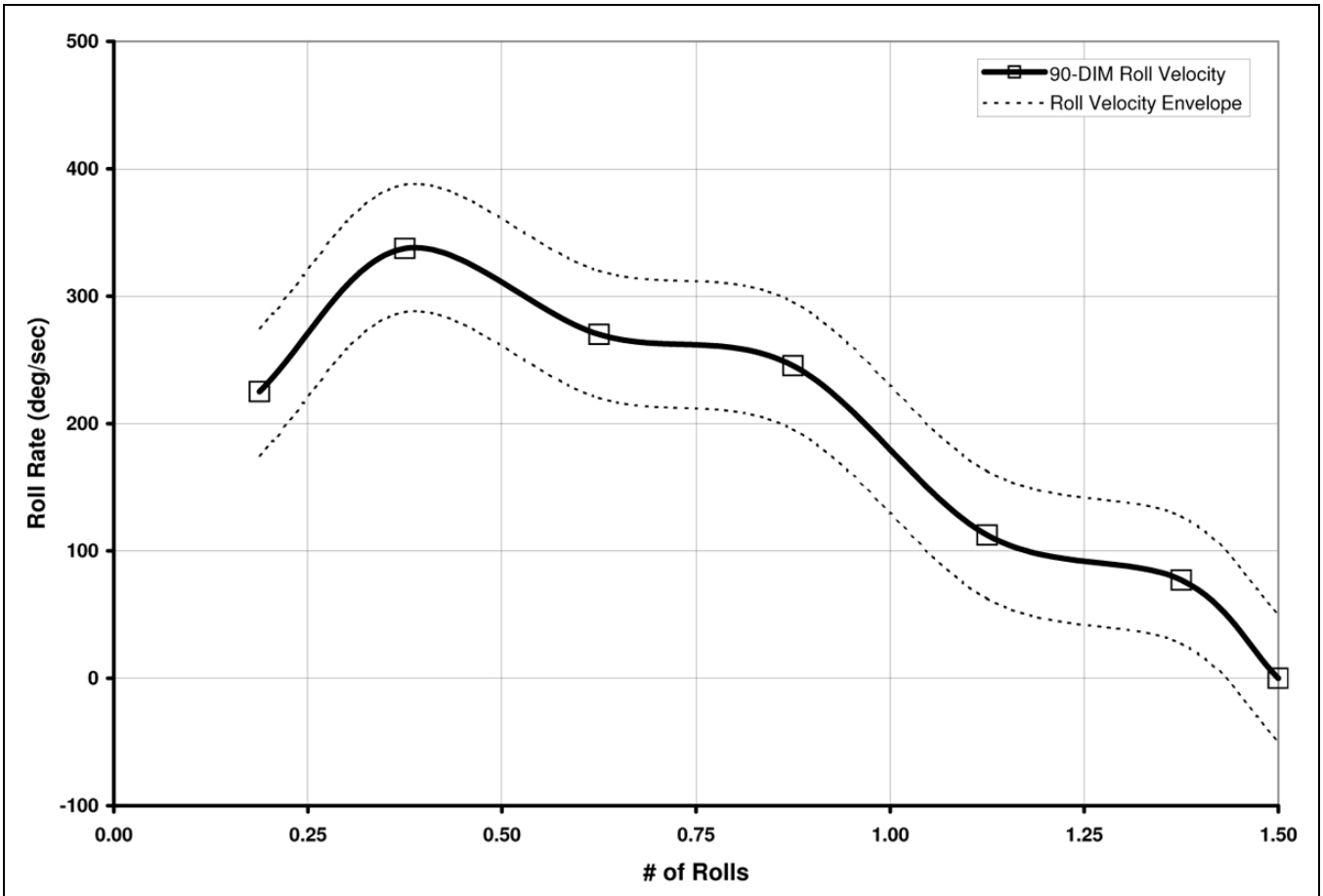


Figure 24 – Roll Velocity v. # of Rolls, Real-World Case #10



Figure 25 – Roll Sequence, Real-World Case #11

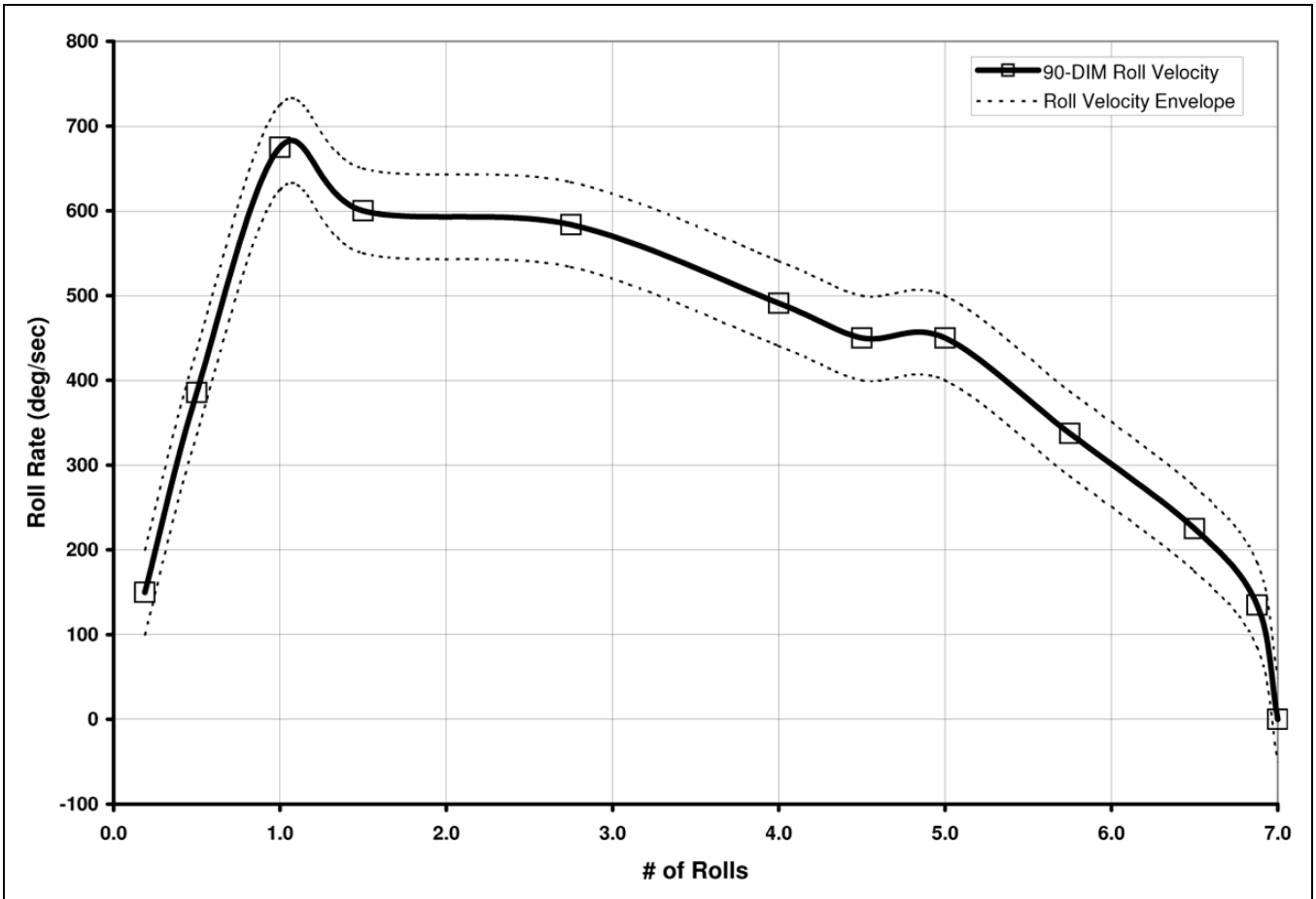


Figure 26 – Roll Velocity v. # of Rolls, Real-World Case #11



Figure 27 – Roll Sequence, Real-World Case #12

PART II – ANALYTICAL MODELING

INTRODUCTION

Part II of this paper introduces two analytical models. The first model is a planar, rigid-vehicle trip phase model. This model is used to explore, in a general sense, the influence that trip force characteristics may exert on the orientation and velocity conditions with which a vehicle enters the roll phase of a rollover accident. The second model is a planar, roof-to-ground impact model. This model is used to explore the influence that the vehicle orientation and velocity conditions will have on the severity of a roof-to-ground impact.

Three main ideas result from consideration of these two models. First, the vehicle orientation and velocity conditions with which the roll phase begins are determined by the characteristics of the trip phase. The characteristics of the trip phase motion are determined by both the vehicle parameters and the trip force characteristics. Second, the initial conditions for the roll phase influence the orientation and velocity conditions that will exist when the vehicle roof impacts the ground. The influence of these initial conditions would be expected to become less discernable the further the vehicle progresses through the roll motion. Third, in conjunction with the velocity conditions that immediately precede the impact, the vehicle orientation that exists when the roof impacts the ground significantly affects the severity of that roof-to-ground impact. Taken together, these three ideas imply that roof-to-ground impact severity will depend, in part, on the trip force characteristics and on the roof-to-ground impact orientations that are realized during the roll phase.

TRIP PHASE MOTION

During the trip phase of a rollover accident, the tripping force causes the vertical load on the vehicle's wheels to vanish, first on the trailing wheels and then on the leading wheels. During the time between leading wheel liftoff and trailing wheel liftoff, the vehicle acquires an upward velocity and a roll velocity and loses a portion of its ground plane velocity.

Following are several examples of tripping mechanisms that can initiate a rollover: (1) interaction between a tire or wheel rim and pavement [6], (2) wheels furrowing into soil or sod [7, 8], and (3) wheels impacting a curb [7, 9]. For each of these mechanisms, the magnitude and duration of the tripping force and the manner in which that force is applied through time will vary. The duration of the trip phase and the speed changes that occur as a result of the trip depend on the characteristics of the trip force [10]. To the extent that the characteristics of the tripping force affect the characteristics of the vehicle motion during the trip phase, each tripping mechanism will produce trip phase vehicle motion characteristic of that mechanism. Of course, the features of the vehicle motion during the trip phase of a rollover would also depend on the vehicle characteristics, such as the weight, moments of inertia, CoM height, track width, and suspension characteristics.

To explore how the trip phase motion varies with the trip force characteristics, this section considers a planar, rigid-vehicle trip phase model. Within this model, the vehicle is subjected, first, to a lateral tripping force that increases linearly with time and, then, to a sinusoidal-shaped tripping force. Figure 28 depicts a free body diagram for the rigid vehicle used in this model. The external forces applied to this vehicle include the vehicle weight, the lateral tripping force, F_T , and the leading side

normal force. The vehicle weight is applied at the CoM and the lateral tripping force and the normal force are applied at the leading side wheels. Figure 28 also depicts the orientation of the fixed coordinate system, which is a right-handed coordinate system with the y-axis pointed to the left and the z-axis pointed up. The angular position of the body is measured with positive rotation in the clockwise direction. With this coordinate system, the vehicle depicted in Figure 26 would be facing into the page and rolling with its passenger's side leading.

Equation (3) describes the angular motion of the vehicle depicted in Figure 28.

$$\alpha_r = \frac{\left(F_T \cdot \delta \cdot c(\lambda - \theta_r) - mg \cdot \delta \cdot s(\lambda - \theta_r) + m \cdot \delta^2 \cdot \omega_r^2 \cdot s(\lambda - \theta_r) \cdot c(\lambda - \theta_r) \right)}{I_{xx} + m \cdot \delta^2 \cdot s^2(\lambda - \theta_r)} \quad (3)$$

In Equation (3), α_r is the roll axis angular acceleration of the vehicle, ω_r is the roll velocity, θ_r is the vehicle roll angle, F_T is the time dependent tripping force, m is the vehicle mass, I_{xx} is the vehicle roll moment of inertia, and g is the gravitational acceleration. Also, in Equation (3), the lower case s and c are used to designate the sine

and cosine, respectively. The geometric parameter, δ , is the distance from the vehicle CoM to the point of the trip force application and is defined as follows:

$$\delta = \sqrt{h^2 + \left(\frac{T}{2}\right)^2} \quad (4)$$

The angle λ is defined as follows:

$$\lambda = \tan^{-1}\left(\frac{T}{2h}\right) \quad (5)$$

Based on these geometric parameters, the roll angle and the roll velocity, Equation (6) yields the vertical velocity at the vehicle CoM, v_z .

$$v_z = \delta \cdot \omega_r \cdot s(\lambda - \theta_r) \quad (6)$$

Equations (3) and (6) will be used below to consider the influence of the trip force characteristics on the vehicle motion. Appendix B contains the full development of these equations.

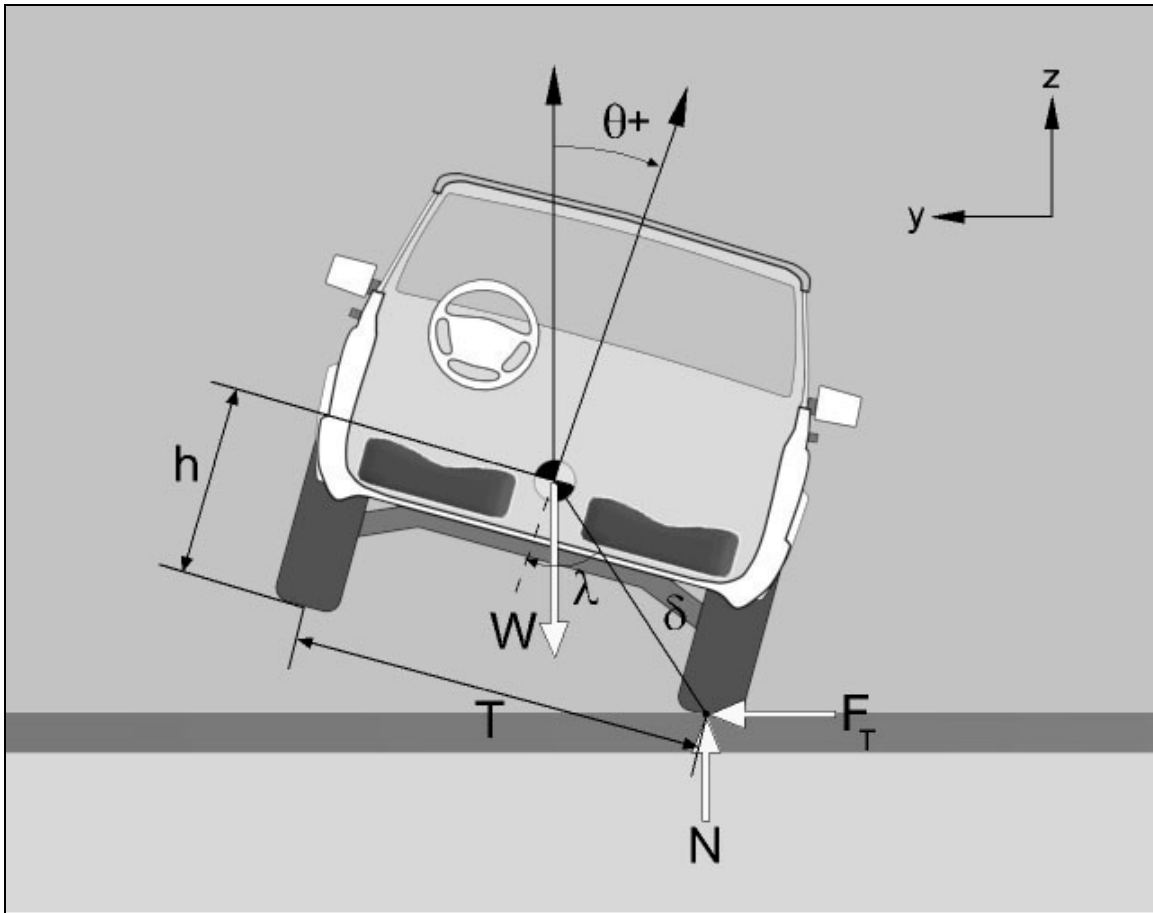


Figure 28 – Free-Body Diagram for a Rigid Vehicle during the Trip Phase

LINEARLY INCREASING TRIP FORCE

Figures 29 and 31 contain roll angle and roll velocity curves obtained by integrating Equation (3) and Figure 33 contains vertical velocity results obtained with Equation (6) for a tripping force that increases linearly with time, as described by Equation (7).

$$F_T(t) = F_0 + (F_{\max} - F_0) \frac{t}{\Delta t_{\text{trip}}} \quad (7)$$

In Equation (7), F_0 is the initial tripping force magnitude, F_{\max} is the maximum tripping force magnitude, Δt_{trip} is the trip duration and t is time. This type of tripping force characteristic may roughly correspond to that which would be produced by a vehicle furrowing into soil, with the force increasing as the depth of the furrowing increases [10, 11]. The results reported in Figures 29, 31 and 33 were produced using the following two vehicle parameter sets:

Vehicle Parameter Set #1 (SUV)

- Vehicle Weight = 5000 lb
- Roll Moment of Inertia = 750 lb-ft-sec²
- Radius of Gyration = 2.2 ft
- Track Width = 61.0 inches
- CoM Height = 28.0 inches

Vehicle Parameter Set #2 (Passenger Car)

- Vehicle Weight = 3600 lb
- Roll Moment of Inertia = 500 lb-ft-sec²
- Radius of Gyration = 2.1 ft
- Track Width = 60.0 inches
- CoM Height = 22.0 inches

The first set of vehicle parameters is representative of a sport utility vehicle and the second is representative of a passenger car. For the results reported in Figures 29, 31 and 33, the trip duration was varied between 0.5 and 1.5 seconds, in ¼ second increments. In all cases, the initial tripping force magnitude was set at the value of the static stability factor and the maximum tripping force magnitude was changed until leading wheel liftoff occurred at the prescribed trip duration.

SINUSOIDAL-SHAPED TRIP FORCE

Figures 30 and 32 contain roll angle and roll velocity curves obtained by integrating Equation (3) and Figure 34 contains vertical velocity results obtained with Equation (6) for a sinusoidal-shaped trip force. This trip force shape is described by Equation (8) as follows:

$$F_T(t) = F_{\max} \sin \left[\pi \frac{t}{\Delta t} \right] \quad (8)$$

This type of trip force shape could reasonably represent an impact-type tripping mechanism where the tripping

force starts out at zero, builds up to a peak value, and then returns to zero. Figures 30, 32 and 34 display results obtained with trip durations between 0.05 and 0.75 seconds. This range starts and ends at lower trip durations than those used for the linearly increasing trip force. The motivation for the low-end of this range is the fact that the sinusoidal-type tripping force would likely be associated with impact-type tripping mechanisms, such as curbs, and would generally occur with short duration applications [9, 12]. The high-end of this range was set so that there would be some overlap between the durations used for the linearly increasing and sinusoidal-shaped trip force shapes. These durations may or may not correspond to real-world trip durations.

Figures 29 through 34 lead to the following observations:

- For both trip force characteristics, the roll angle at the end of the trip phase increased with increasing trip duration.¹ In all cases, the passenger car achieved higher roll angles during the trip phase than the SUV. The linearly increasing trip force resulted in a greater difference in roll angle between the passenger car and SUV than did the sinusoidal trip force.
- For both trip force characteristics, the roll velocity at the end of the trip phase decreased with increasing trip duration. In all cases, the passenger car achieved higher roll rates than the SUV. The linearly increasing trip force resulted in higher roll rates for a given trip duration than the sinusoidal trip force. The linearly increasing trip force resulted in greater roll rate differences between the passenger car and the SUV than did the sinusoidal trip force.
- For both trip force characteristics, the vertical velocity curves peaked prior to the end of the trip phase. The vertical velocity then dropped off before leading wheel liftoff occurred. The magnitude of difference between the peak vertical velocity and the vertical velocity at leading wheel liftoff depended on the trip force shape and duration and on the vehicle parameters. The passenger car achieved higher vertical velocities during the trip phase than the SUV. The linearly increasing trip force resulted in higher vertical velocities than the sinusoidal trip force.
- The sinusoidal trip force resulted in a peak vertical velocity that occurred earlier in time than for the linearly increasing trip force. The sinusoidal trip force also resulted in a greater vertical velocity drop between the peak and the vertical velocity at leading wheel liftoff.

¹ For a sinusoidal trip force with a short duration trip phase, leading wheel liftoff occurs at very low roll angles. This being the case, leading wheel lift-off may be an inadequate definition of the end of the trip phase in these cases because it is possible that one could see the leading wheel come unloaded without the vehicle continuing to roll.

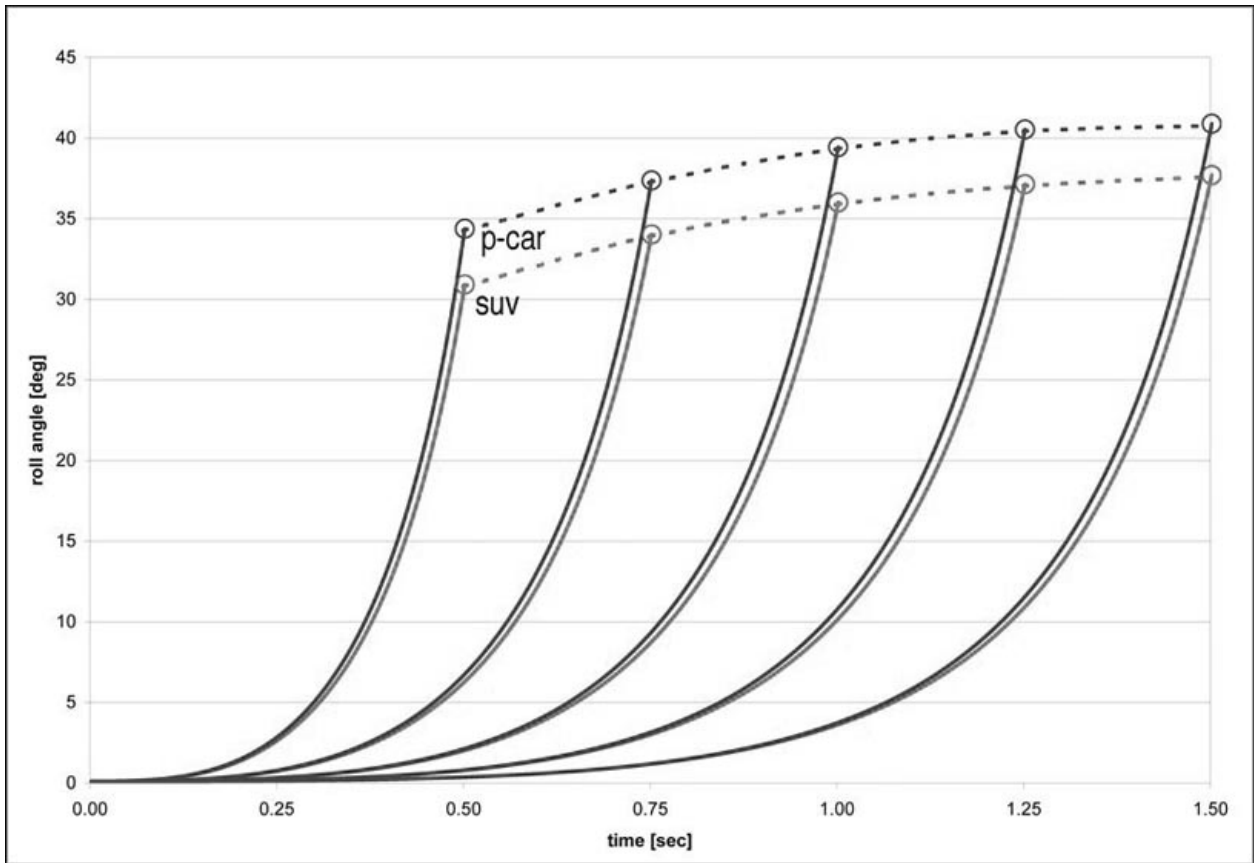


Figure 29 – Roll Angle v. Time, **Linearly Increasing Trip Force**, Varying Trip Durations

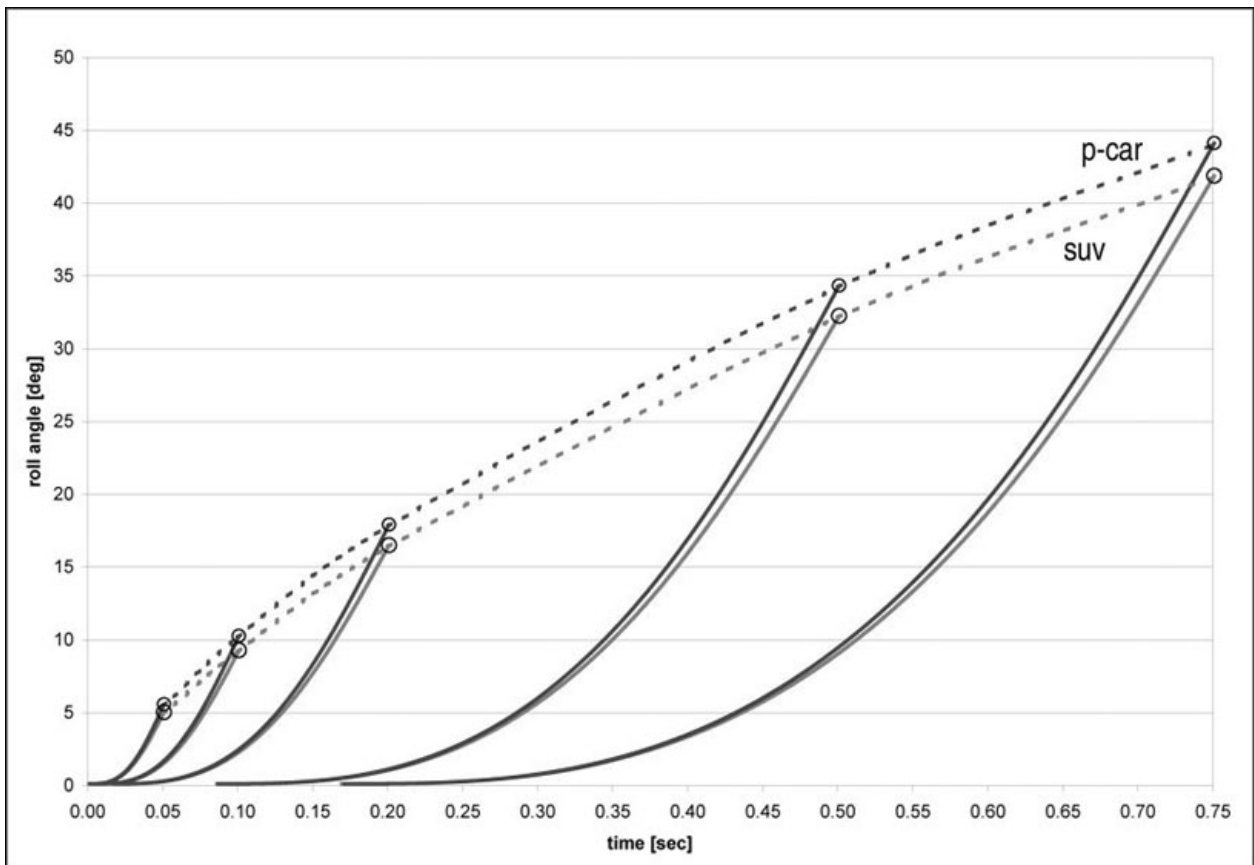


Figure 30 – Roll Angle v. Time, **Sinusoidal-Shaped Trip Force**, Varying Trip Durations

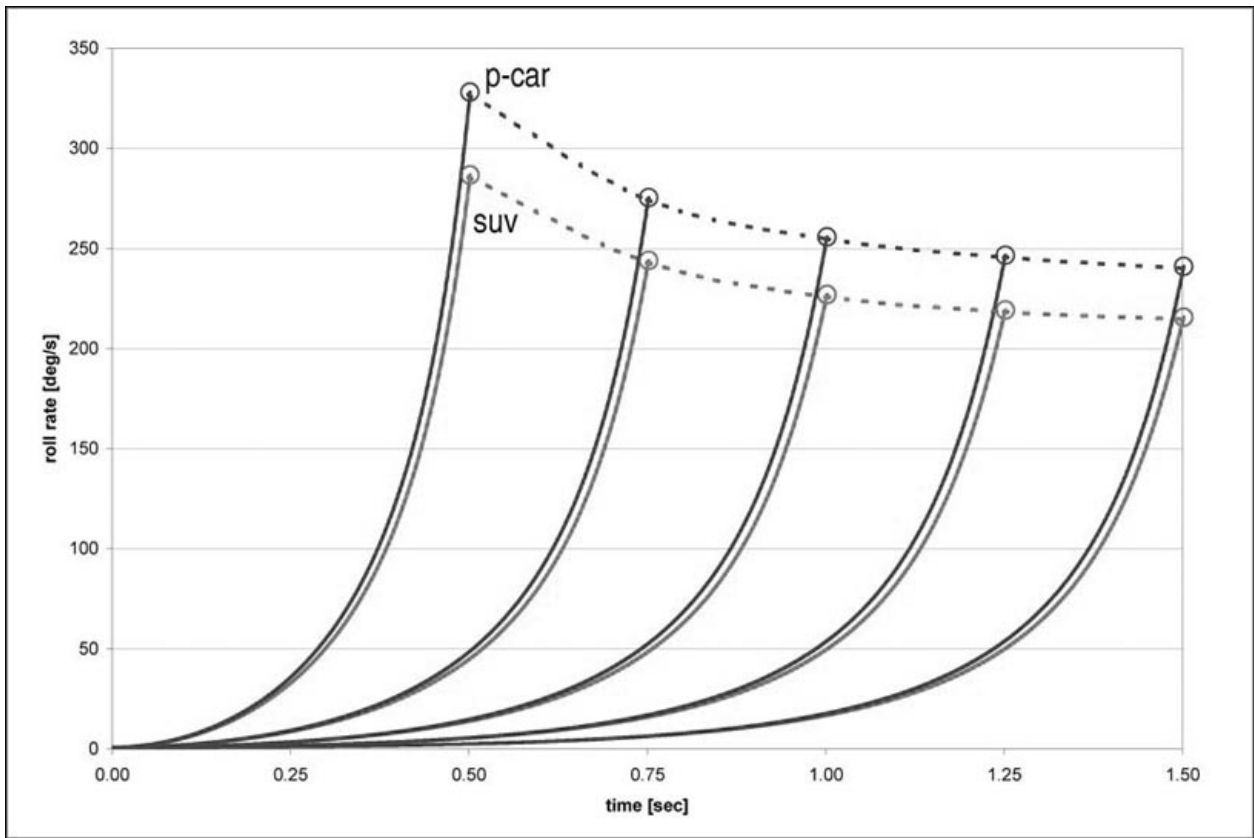


Figure 31 – Roll Rate v. Time, Linearly Increasing Trip Force, Varying Trip Durations

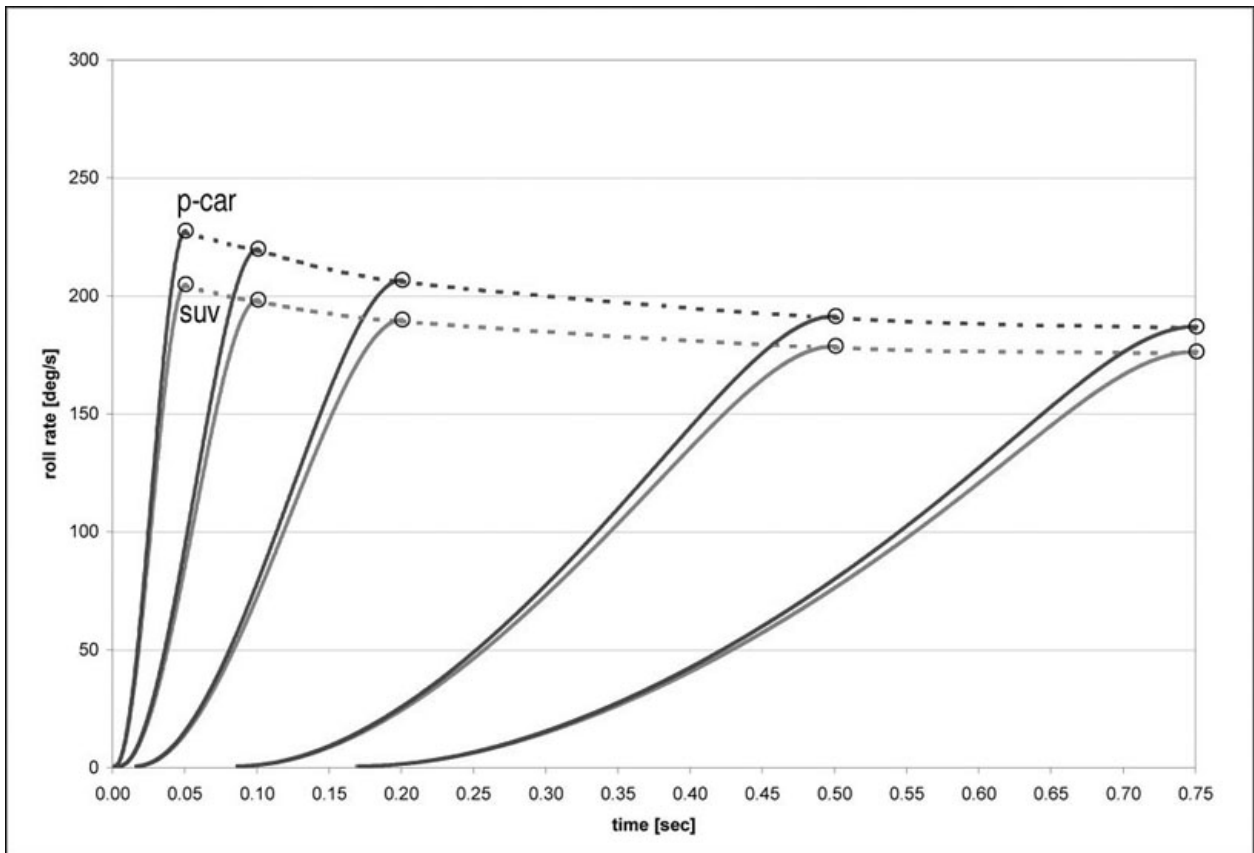


Figure 32 – Roll Rate v. Time, Sinusoidal-Shaped Trip Force, Varying Trip Durations

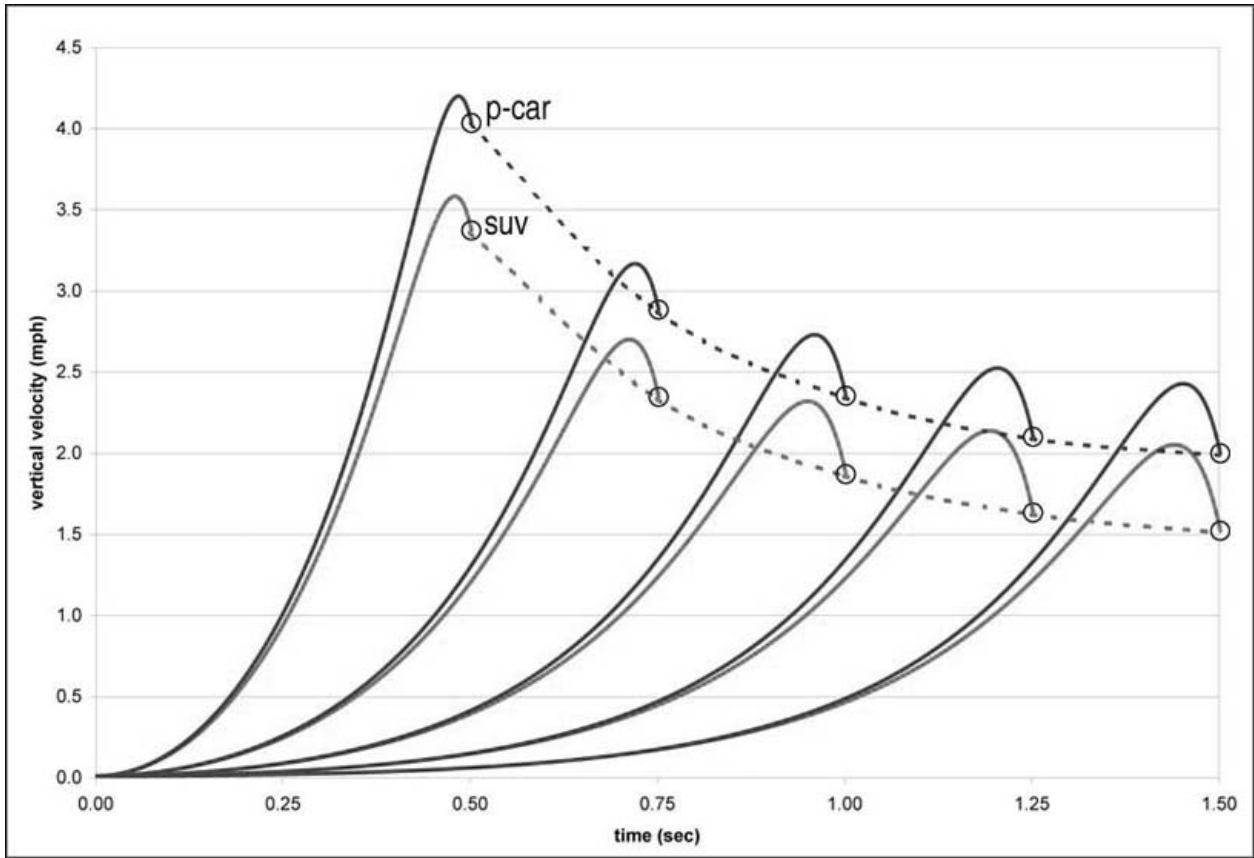


Figure 33 – Vertical Velocity v. Time, **Linearly Increasing Trip Force**, Varying Trip Durations

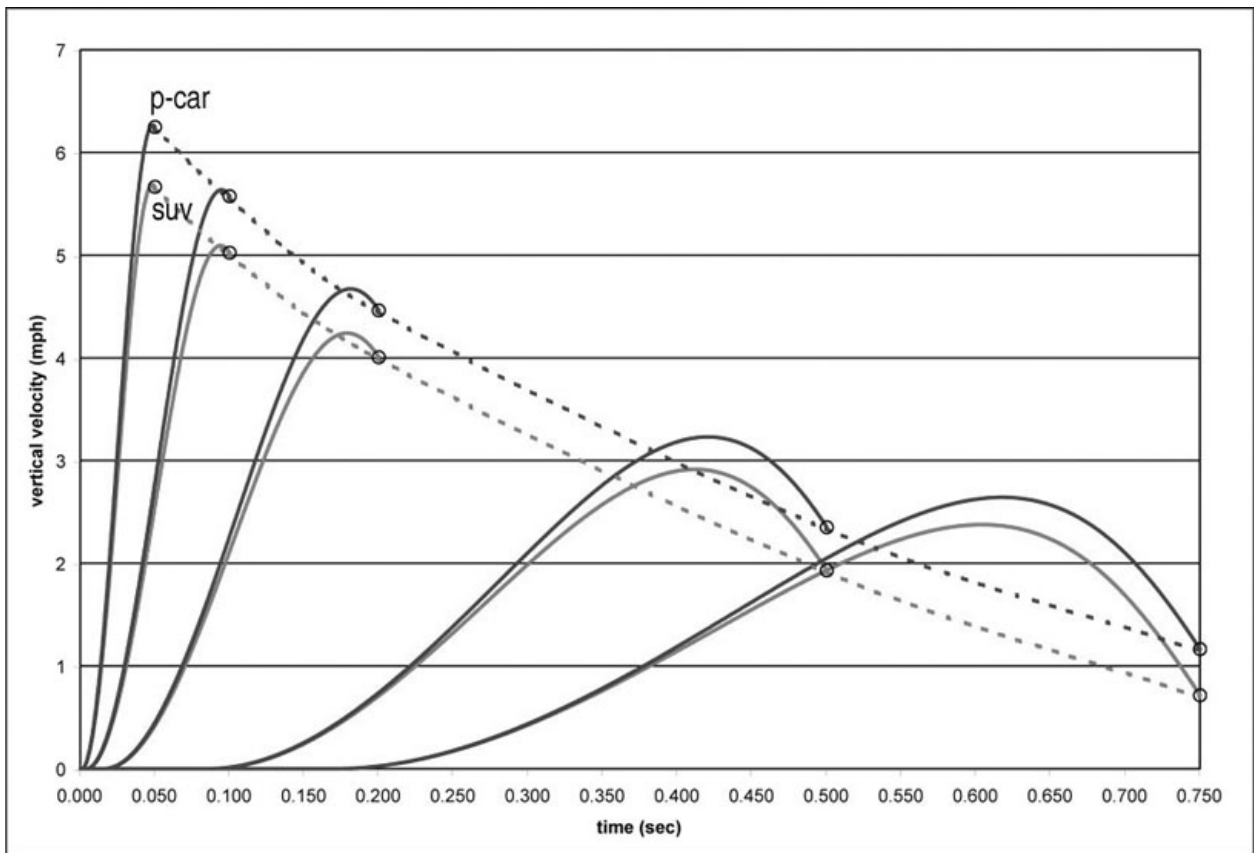


Figure 34 – Vertical Velocity v. Time, **Sinusoidal-Shaped Trip Force**, Varying Trip Durations

These results demonstrate that the vehicle orientation and velocity conditions that exist when a vehicle enters the roll phase depend on both the vehicle characteristics and the trip force characteristics. In all cases, the passenger car configuration resulted in higher roll angles, roll rates and vertical velocities than the SUV. Beyond that, the velocity conditions that existed at the end of the trip phase varied with varying trip force characteristics. It stands to reason that the vehicle motion that occurs during the roll phase will depend on the orientation and velocity conditions with which the vehicle enters that phase. Therefore, the trip force characteristics will be influential in determining the vehicle motion that will occur during the roll phase. This is not to say that there will be a discernable relationship between the initial conditions for the roll phase and the roll motion that results. Generally, there will be a clear relationship between these initial conditions and the first roof-to-ground impact. After contact occurs between the roof and the ground, the relationship between the initial conditions for the roll phase and the resulting motion will become less discernable because subsequent vehicle-to-ground contacts also become influential in the subsequent motion.

ROOF-TO-GROUND IMPACT SEVERITY

Figure 35 depicts a planar impact between a vehicle roof and the ground. In this figure, the vehicle is depicted with translational velocity both along and into the ground plane and with a positive roll velocity. In this model, the collision impulse is assumed to be transferred instantaneously at the Point C. This impulse has components P_y and P_z . Figure 35 also includes a gravity impulse, designated at P_g . Within most planar impact models for vehicle-to-vehicle impacts, external impulses acting on the vehicle are negligible relative to the collision impulse and can be neglected. That will not necessarily be the case for a roof-to-ground impact, and so, the impulse from gravity is included in the impact model equations. Using the principle of impulse and momentum, one can derive Equations (9) through (11), which yield the CoM velocity changes and the change in roll velocity that would occur during the impact of Figure 35.

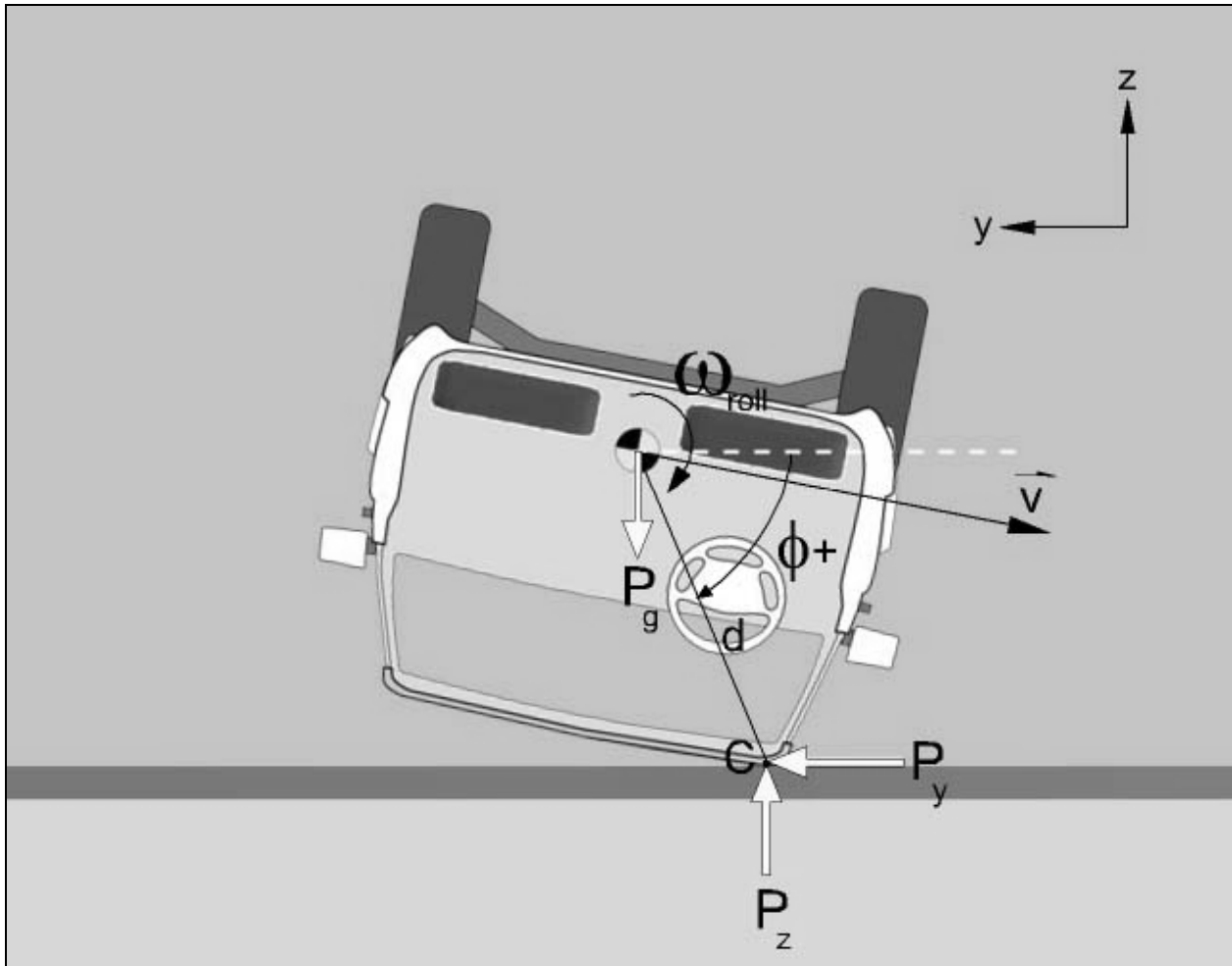


Figure 35 – Planar Roof-to-Ground Impact

$$\Delta V_z = - \left[\begin{array}{l} (1+e) \cdot v_{zc,i} \cdot \left\{ \frac{k_r^2}{k_r^2 + d^2(c^2\phi - \mu \cdot s\phi \cdot c\phi)} \right\} + \\ g \cdot \Delta t_i \cdot \left\{ \frac{d^2(c^2\phi - \mu \cdot s\phi \cdot c\phi)}{k_r^2 + d^2(c^2\phi - \mu \cdot s\phi \cdot c\phi)} \right\} \end{array} \right] \quad (9)$$

$$\Delta V_y = \mu \cdot \Delta V_z \quad (10)$$

$$\Delta \omega_r = -(\Delta V_z + g \cdot \Delta t_i) \cdot \frac{d \cdot (c\phi - \mu \cdot s\phi)}{k_r^2} \quad (11)$$

In Figure 35 and Equations (9) through (11), k_r is the vehicle's radius of gyration for the roll axis, d is the distance between the vehicle CoM and Point C, ϕ is the orientation of the line connecting the CoM to the Point C, measured as depicted in Figure 35, $v_{zc,i}$ is the vertical velocity of Point C immediately preceding the ground contact, g is the gravitational constant, and Δt_i is the duration of the impact. It is important to note here that although the collision impulse is assumed to be transferred instantaneously, the inclusion of the gravity impulse requires the impact duration to be estimated.

The vertical velocity at Point C immediately preceding the ground impact, $v_{zc,i}$, is related to the CoM vertical velocity, the roll velocity and the roll angle immediately preceding the contact. This velocity is given by Equation (12). In this equation v_{zi} is the vertical velocity of the CoM immediately preceding the impact.

$$v_{zc,i} = v_{zi} - d \cdot \omega_{r,i} \cdot c\phi \quad (12)$$

Equations (9) through (11) also utilize the coefficient of restitution, e , and the impulse ratio, μ , which govern the impact energy loss along the vertical and ground plane directions. The impulse ratio should not be thought of as a coulomb friction value that simply governs the sliding force between the vehicle body and the ground. Rather, this quantity is the ratio of the ground plane impulse to the vertical direction impulse. In addition to the effects of friction between the ground and the vehicle body, the ground plane impulse may also include the effects of forces generated by snagging between the vehicle body and the ground. This impulse can cause deformation to the roof structure from forces that exceed purely frictional forces. One can obtain an equation that yields a critical impulse ratio at which the velocity of the Point C will go to zero during the impact. This critical impulse ratio will depend on the CoM velocity conditions and on the roll velocity and thus, the significance of any value of the impulse ratio will also depend on the specific velocity conditions of the vehicle immediately preceding the impact.

In addition to the CoM velocity changes, the velocity changes at the roof-to-ground contact point may have significance to assessing the severity of a roof-to-ground

impact for the roof structure and for the occupants. Equations (13) and (14) yield the ground plane and vertical component of the velocity change that would occur at the roof-to-ground contact point, C, depicted in Figure 35.

$$\Delta V_{y,c} = \Delta V_y + d \cdot s\phi \cdot \Delta \omega_r \quad (13)$$

$$\Delta V_{z,c} = \Delta V_z - d \cdot c\phi \cdot \Delta \omega_r \quad (14)$$

Equations (9) through (14) are derived with the principle of impulse and momentum. As with other impact models derived with this principle, these equations assume, first, that the impact force is transferred instantaneously and, second, that the impact force can be idealized as being applied at a single point. The accuracy of these assumptions depends on the duration over which a roof-to-ground impact occurs and on how much of the roof structure is involved in the impact. Some roof-to-ground contacts have a sustained duration during which the vehicle rolls through a significant angle. In such cases, assuming an instantaneous, isolated force transfer may be inaccurate. At other times, the roof-to-ground contact will be short and isolated to one area of the roof structure, such that these assumptions can be reasonably invoked.

The duration of a roof-to-ground impact will be determined by a number of factors, including the vehicle's translational and angular velocity conditions immediately preceding the impact [13], the orientation with which the vehicle impacts the ground, and by the stiffness of the roof structure. Generally speaking, for a fixed impact orientation, the impact duration would be expected to decrease as the vehicle's roll rate and roof stiffness increase. This is the point at which the structural properties of the roof would enter into this modeling.

As with any other impact type to which an instantaneous force transfer impact model is applied, the analyst would need to determine the most representative time at which to define the impact – the instant in time that would best represent the force application that actually occurs over a finite time period. The most representative time would be influenced by the impact duration, which would, in part, be determined by the stiffness of the roof. Thus, the orientation angle, ϕ , should not necessarily be taken as the orientation when the roof first impacts the ground, but rather as the orientation when the resultant collision force is transferred. Additional research would be necessary to determine how this angle would be defined in practice.

For now, it is adequate to consider Equations (9) through (14) conceptually, since they allow for the identification of trends and principles related to the severity of roof-to-ground impacts. Specifically, by examining Equations (9) through (14), the following observations can be made:

- For a given impact orientation, there is a direct relationship between the downward roof velocity and the vertical and angular velocity changes that occur during that impact. Increasing the downward roof velocity translates to increasing velocity changes.
- For a vehicle with a given CoM downward velocity and a given roll velocity, the downward velocity with which the roof actually impacts the ground depends on the vehicle orientation.
- The velocity changes realized during a particular roof-to-ground impact is related to the vehicle orientation at impact in a highly non-linear fashion.
- The magnitude of the velocity changes that are realized for a given downward roof velocity depend on the relative magnitude of k_{roll} and d .

Now, consider how the velocity changes of Equations (9) through (14) translate to energy loss during the impact. The energy loss during the impact depicted in Figure 35 can be written as follows:

$$E_d = \frac{1}{2}m(v_{zi}^2 - v_{zf}^2 + v_{yi}^2 - v_{yf}^2 + k_r^2\{\omega_{r,i}^2 - \omega_{r,f}^2\}) \quad (15)$$

This equation accounts for CoM velocity changes in the vertical and ground plane directions and for a change in roll velocity. In fact, Equation (15) can be rewritten in terms of the CoM vertical velocity change, the roll velocity change, and the initial velocity conditions as follows:

$$E_d = -\frac{1}{2}m \left[\Delta V_z^2(1 + \mu^2) + 2\Delta V_z(v_{zi} + \mu v_{gi}) + k_r^2\Delta\omega_r(2\omega_{r,i} + \Delta\omega_r) \right] \quad (16)$$

The energy loss quantified by Equation (16) includes both the energy loss due to vehicle deformation, the energy loss due to sliding and snagging between the vehicle structure and the ground, and the energy dissipated by the ground. Assuming the ground absorbs a negligible amount of energy and that the ground plane impulse does not deform the roof structure, then the energy that the vehicle roof structure is called on to absorb through deforming can be estimated by calculating the work done by the vertical direction impulse during the impact. As shown in Appendix C, this calculation results in Equation (17).

$$E_{d,z} = -\frac{1}{2}m \cdot (1 - e) \cdot v_{zc,i} \cdot (\Delta v_z + g\Delta t_i) \quad (17)$$

There will be many cases when the ground will absorb a substantial quantity of energy and when the ground plane impulse will deform a vehicle's roof structure. In

these cases, Equation (17) will not accurately characterize the deformation energy for the impact.

Now, consider the effect of the vehicle orientation on the ground impact severity with two sets of hypothetical impacts. Using the inertial properties from the SUV parameter set used in the previous section, suppose that the vehicle has a ground plane velocity of 40 mph and a downward CoM velocity of 3 mph. For the first set of impacts, assume that the vehicle has a roll velocity of 200 degrees per second and experiences an increase in roll velocity during the impact. This type of situation would likely occur during the first or second roll of a multi-roll accident. In addition to these velocity conditions, assume that 3-1/2 feet separate the CoM and the roof-to-ground contact point, that the impact has a coefficient of restitution of 0.100 and an impulse ratio of 0.7, and that it has a duration of 30 milliseconds. An impulse ratio of 0.7 was chosen to generate an increase in roll velocity consistent with those discussed in Part I. Given these conditions, Table 2 lists the velocity changes and energy dissipation that occur for a range of vehicle orientation angles (ϕ).

For the second set of impacts, assume that the vehicle has a roll velocity of 450 degrees per second and experiences a decrease in roll velocity. This type of impact would generally occur downstream of the first roll during a multi-roll accident. In this case, the impulse ratio is set equal to a value of 0.05. This impulse ratio was chosen to produce a roll velocity decrease consistent with those discussed in Part I. Table 3 lists the velocity changes and energy dissipation that occur for a range of vehicle orientation conditions under these velocity conditions. It should be noted that the impacts of both Tables 2 and 3 would be considered trailing side impacts, meaning that the area of the roof that is impacting the ground in these cases would have been initially trailing during the trip phase.

The values reported in Tables 2 and 3 demonstrate that the severity of a particular roof-to-ground impact is highly dependent on the vehicle orientation. With identical velocity conditions, orientations of 65 and 95 degrees produced vastly different severities. For the impacts of Table 2, the vehicle with an orientation of 65 degrees experiences a CoM velocity change of 11.6 mph, a roof-to-ground contact point velocity change of 13.2 mph, and an increase in roll velocity of 114 degrees per second. At an orientation of 95 degrees, the vehicle experiences only a 2.5 mph CoM velocity change, a 4.7 mph roof-to-ground contact point velocity change and a 66 degree per second increase in roll velocity. The total energy loss for the impact at 65 degrees was 69,112 foot-pounds, whereas at 95 degrees it was only 16,548 foot-pounds. For these impacts, a substantial portion of the energy loss is caused by the ground plane impulse. This being the case, no attempt was made in Table 2 to estimate the roof deformation energy.

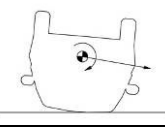
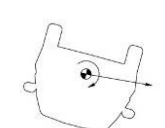
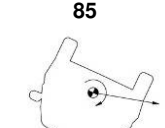
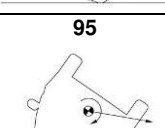
CoM Velocity Conditions (Ground Plane Velocity = 40 mph, Downward Velocity = 3 mph, Roll Velocity = 200 deg/s)	Vehicle Orientation, ϕ (deg)	Downward Velocity at Roof Contact Point (mph)	Vertical Velocity Change (mph)		Total Velocity Change (mph)		Change in Roll Velocity (deg/s)	Energy Dissipated by the Impact (ft-lb)	Estimated Roof Deformation Energy (ft-lb)
			Center of Mass	Roof-to-Ground Contact Point	Center of Mass	Roof-to-Ground Contact Point			
	65	6.5	9.5	7.5	11.6	13.2	114	69,112	-
	75	5.2	8.1	6.0	9.8	14.5	188	54,681	-
	85	3.7	4.8	4.3	5.9	10.7	155	33,448	-
	95	2.3	2.0	2.3	2.5	4.7	66	16,548	-

TABLE 2 – SUV Roof-to-Ground Impacts, Identical CoM Velocity Conditions, Varying Orientations, Positive $\Delta\omega$

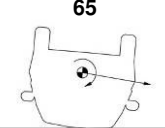
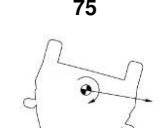
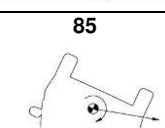
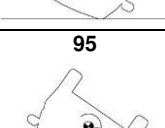
CoM Velocity Conditions (Ground Plane Velocity = 40 mph, Downward Velocity = 3 mph, Roll Velocity = 450 deg/s)	Vehicle Orientation, ϕ (deg)	Downward Velocity at Roof Contact Point (mph)	Vertical Velocity Change (mph)		Total Velocity Change (mph)		Change in Roll Velocity (deg/s)	Energy Dissipated by the Impact (ft-lb)	Estimated Roof Deformation Energy (ft-lb)
			Center of Mass	Roof-to-Ground Contact Point	Center of Mass	Roof-to-Ground Contact Point			
	65	10.9	8.4	11.5	8.4	13.1	-177	16,880	14,813
	75	7.8	7.5	8.5	7.5	9.0	-88	11,251	9,638
	85	4.6	5.0	5.1	5.1	5.1	-10	5,182	3,977
	95	1.4	1.4	1.5	1.4	1.5	7	1,384	431

TABLE 3 – SUV Roof-to-Ground Impacts, Identical CoM Velocity Conditions, Varying Orientations, Negative $\Delta\omega$

For the impacts of Table 3, the vehicle with an orientation of 65 degrees experiences a CoM velocity change of 8.4 mph, a roof-to-ground contact point velocity change of 13.1 mph, and a decrease in roll velocity of 177 degrees per second. At an orientation of 95 degrees, the vehicle experiences only a 1.4 mph CoM velocity change, a 1.5 mph roof-to-ground contact point velocity change and a slight increase in roll velocity of 7 degrees per second. The total energy loss for the impact at 65 degrees was 16,880 foot-pounds, whereas at 95 degrees it was only 1,384 foot-pounds.

For the impacts of both Tables 2 and 3, the 65 degree impact orientation resulted in a much more severe impact than the 95 degree orientation. In contrast to the impacts of Table 2, the ground plane impulse had little effect on the velocity changes and energy loss for the impacts of Table 3.

Thus, the impacts of these tables have the following implications: (1) The direction of the impact force during a trailing side impact depends on the impact velocity conditions and on the change in roll velocity that occurs during the impact. Impacts resulting in an increase in roll velocity would have a larger ground plane component than those that result in a decrease in roll velocity. (2) Generally speaking, roof-to-ground impacts that result in an increase in roll velocity would occur early in a roll sequence, whereas roof-to-ground impacts that result in a decrease in roll velocity would occur later in a roll sequence. Thus, the impacts in Tables 2 and 3 demonstrate that severe roof-to-ground impacts could occur at any point during the roll sequence. (3) However, the direction of force associated with a specific roof-to-ground impact may depend on the portion of the roll sequence in which that impact occurs.

To give greater meaning to the deformation energy values of Table 3, consider how these energy values might compare to the energy that a roof structure would be called upon to absorb during a hypothetical FMVSS 216 test. In an FMVSS 216 test, a flat plate is used to apply a force to the roof structure that has a magnitude of 1-1/2 times the unloaded vehicle weight. Under this loading, the roof structure must not deform more than 5 inches. A typical force-deformation curve for a 216 test can be approximated using the force-saturation model shown in Figure 36 [14, 15, 16]. For the force-deformation curve shown in this figure, the force increases linearly with deformation until the force saturates at a deformation depth equal to C_{SAT} and a force level equal to F_{peak} . At this point the force level remains constant up until the maximum deformation depth, C_{max} , is reached.

The energy absorbed by the roof structure during a 216 test can be obtained by calculating the area underneath the force-deformation curve. For the idealized force-deformation curve of Figure 36, the absorbed energy is given by the following equation:

$$E_A = F_{peak} \left(C_{max} - \frac{C_{SAT}}{2} \right) \quad (20)$$

For a typical 216 test, the peak force occurs at a deformation level between 2 and 3 inches [14, 15, 16]. Again using the SUV parameter set and assuming that, at 3 inches, the roof structure for this vehicle achieved the strength-to-weight ratio required in the 216 test, the roof structure of this vehicle would absorb approximately 2,188 ft-lb during the 216 test. This calculation assumes that the roof structure ultimately deformed the 5 inches allowed in the 216 test.

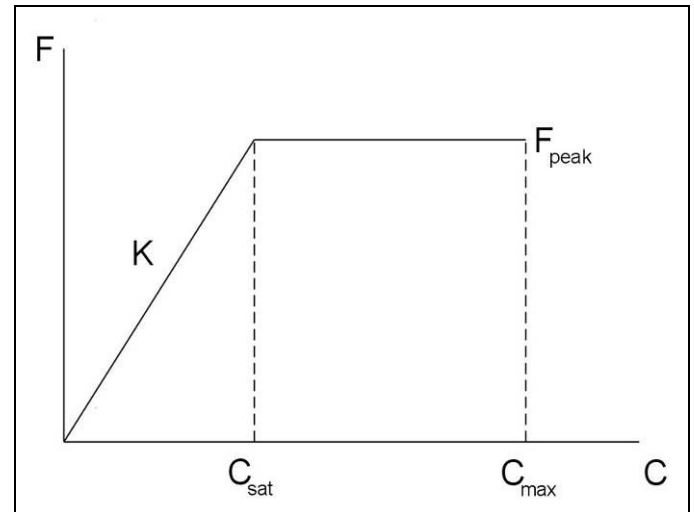


Figure 36 – Idealized Force-Deformation Curve for FMVSS 216 Test

A roof structure generally has greater energy absorption capabilities under dynamic impact loading than under the quasi-static loading of a 216 test [14]. Thus, a roof that experiences a deformation of 5 inches during a roof-to-ground impact will reach a higher force level and will accomplish greater energy absorption than the same roof experiencing 5 inches of deformation in a 216 test. Rains found that under dynamic loading, roofs generally absorb between 10 and 60 percent more energy than under static loading. Thus, a roof structure that absorbed 2,188 ft-lb during a 216 test would have the capacity to absorb between 2,406 and 3,500 ft-lb of energy under dynamic loading, while limiting the roof deformation to 5 inches.

Comparing these values to the deformation energy values of Table 2 reveals that, with an impact orientation of 65 degrees, the energy absorption capacity demanded by the impact would exceed the energy absorption capacity demanded by this hypothetical 216 test by 4.2 to 6.2 times. If the A-pillar/header area of the roof were called on to absorb this entire energy in a manner similar to a 216 test, this portion of the roof would require a strength-to-weight ratio between 6.3 and 9.2. On the other hand, at an orientation of 95 degrees, the roof would require only a small fraction of the energy absorption capacity that it would in a 216 test. Of course,

it should be stated that how the absorption of energy by the roof structure translates to deformation depends on a number of factors, including the specific structures of the roof that are engaged, the surface area over which the impact force is applied and the impact duration. Nonetheless, it again becomes clear that for fixed velocity conditions, the impact severity depends heavily on the impact orientation.

The numerical results reported in Tables 2 and 3 are, of course, illustrative values calculated with representative vehicle parameters and representative velocity conditions that could occur during a rollover accident. Such values could potentially be calculated for a specific vehicle in a specific crash. These calculations would need to utilize a reconstruction of the roll phase for that specific accident and inertial parameters representative of the specific vehicle involved. In many cases, these calculations would also need to include the three-dimensional nature of the roof-to-ground impact under consideration. Such calculations could result in values both lower and higher than those represented in Tables 2 and 3. Further research could explore rollover crash tests to examine appropriate values for the impact model used here and to explore the limits of its applicability.

CONCLUSIONS

REAL-WORLD ROLLOVER ANALYSIS

The research reported in Part I of this paper resulted in the following conclusions:

- The video analysis method used in this paper employed 90-degree roll angle intervals to generate roll rate time histories. Despite this relatively large sampling interval, this method will result in roll rate time histories that generally lie within ± 50 degrees per second of the actual roll rate time history.
- The video analysis method employed in this paper results in considerable smoothing of the actual roll rate time histories. Thus, significant changes in roll velocity that occur over short durations in the actual roll rate time history occur over much longer durations in the roll rate time histories obtained with the video analysis method.
- For the twelve rollover accidents analyzed, the video analysis yielded initial roll rates between 150 and 540 degrees per second.
- The video analysis method yielded peak roll rates for these rollovers that varied between 300 and 675 degrees per second. These roll rates appeared highly dependent on the specific vehicle-to-ground impacts that were realized during the roll sequence.
- The video analysis method yielded peak roll rates during the times that the vehicles in these rollovers

were on their roofs that varied between 300 and 600 degrees per second.

- The video analysis method yielded average roll velocities for these rollover accidents that varied between 144 degrees per second and 395 degrees per second.
- Vehicle-to-ground impacts that resulted in significant increases in roll velocity tended to occur early in the roll sequence whereas vehicle-to-ground impacts that resulted in significant decreases in roll velocity tended to occur later in the roll sequence. In all but one of the twelve cases, the first roll accelerated the roll velocity such that the peak roll velocity occurred downstream of the first roll.

The research reported in Part II of this paper resulted in the following conclusions:

TRIP PHASE MODELING

- The characteristics of the trip force that initiates a rollover will, in part, determine the orientation and velocity conditions with which a vehicle enters the roll phase.
- The vehicle parameters will also be influential in determining the orientation and velocity conditions with which the vehicle enters the roll phase. In all of the scenarios considered in this paper, a passenger car configuration resulted in higher roll angles, roll velocities, and vertical velocities at the beginning of the roll phase than did a sport utility vehicle configuration.
- The vehicle orientation and velocity conditions that exist at the time the vehicle enters the roll phase are factors influencing the severity of the roof-to-ground impacts that will occur during the rollover. These conditions will most directly influence the severity of the first roof-to-ground impact.

ROOF-TO-GROUND IMPACT MODELING

- The severity of a roof-to-ground impact is determined by factors such as the vehicle's velocity conditions at impact, the orientation when the resultant collision force is transferred and the vehicle inertial properties.
- Severe roof-to-ground impacts are associated with either significant increases or significant decreases in roll velocity.
- Severe roof-to-ground impacts can occur during any portion of the roll sequence of a multi-roll accident. This statement is based on the observation that significant changes in roll velocity can occur throughout the roll sequence.

- The direction of force that results from a specific roof-to-ground impact will depend on the impact velocity conditions, the vehicle orientation at impact and the vehicle inertial properties. Roll velocity increases and roll velocity decreases will be associated with different force directions relative to the ground plane.

REFERENCES

1. Hughes, Raymond J., "A Dynamic Test Procedure for Evaluation of Tripped Rollover Crashes," Paper Number 2002-01-0693, SAE, Warrendale, PA, 2002.
2. Mills, P.J., Hobbs, C.A., "Probability of Injury to Car Occupants in Frontal and Side Impacts," 841652, Society of Automotive Engineers, Warrendale, PA, 1984.
3. Digges, Kennerly, Eigen, Ana Maria, "Severity Measurements for Rollover Crashes."
4. "Spline (mathematics)." Wikipedia, The Free Encyclopedia. 10 Nov 2006, 21:13 UTC. Wikimedia Foundation, Inc. 9 Jan 2007
<http://en.wikipedia.org/w/index.php?title=Spline_%28mathematics%29&oldid=87012780>.
5. Steffan, Hermann and Moser, Andreas, "How to Use PC-Crash to Simulate Rollover Crashes," 2004-01-0341, Society of Automotive Engineers, Warrendale, PA, 2004.
6. Marine, Micky C., Thomas, Terry M., Wirth, Jeffrey L., "Characteristics of On-Road Rollovers," 1999-01-0122, Society of Automotive Engineers, Warrendale, PA, 1999.
7. Cooperrider, Neil K., Thomas, Terry M., Hammoud, Selim A., "Testing and Analysis of Vehicle Rollover Behavior," 900366, Society of Automotive Engineers, Warrendale, PA, 1990.
8. Cooperrider, Neil K., Hammoud, Selim A., Colwell, Jeff, "Characteristics of Soil-Tripped Rollovers," 980022, Society of Automotive Engineers, Warrendale, PA, 1998.
9. Jones, Ian S., "The Mechanics of Rollover as a Result of Curb Impact," 750461, Society of Automotive Engineers, Warrendale, PA, 1975.
10. Orlowski, K.F., Moffatt, E.A., Bundorf, R.T., Holcomb, M.P., "Reconstruction of Rollover Collisions," 890857, Society of Automotive Engineers, Warrendale, PA, 1989.
11. Gopal, Madana, Baron, Ken, Shah, Minoo, "Simulation and Testing of a Suite of Field Relevant Rollovers," 2004-01-0335, Society of Automotive Engineers, Warrendale, PA, 2004.
12. Shi, Yibing, Nusholtz, Guy S., "Simple Models for Analysis of Curb- and Soil-trip Rollover Events," 2006-01-0722, Society of Automotive Engineers, Warrendale, PA, 2006.
13. Moffatt, Edward A., Submission to NHTSA Docket Number 1999-5572, December 4, 2001.
14. Rains, Glen C., "Quasi Static and Dynamic Roof Crush Testing," NHTSA, VRTC-82-0197/VRTC-86-0391.
15. Wilke, Donald T., "Status of NHTSA's Roof Crush Research," Presentation at SAE Government/Industry Meeting, May 10, 2004.
16. FMVSS 216, Upgrade, Roof Crush Resistance, Office of Regulatory Analysis and Evaluation, August 2005.
17. Brach, Raymond M., Brach, R. Matthew, Vehicle Accident Analysis and Reconstruction Methods, SAE, 2005.

CONTACT

The authors welcome questions and comments related to the research reported in this paper. The video clips analyzed for this paper are available from the authors upon request.

Contact Information:

Kineticorp, LLC
44 Cook St., Suite 510
Denver, CO 80206
(303) 733-1888
www.kineticorp.com

APPENDIX A – ADDITIONAL ROLL CURVES FOR VIDEO ANALYSIS METHODOLOGY

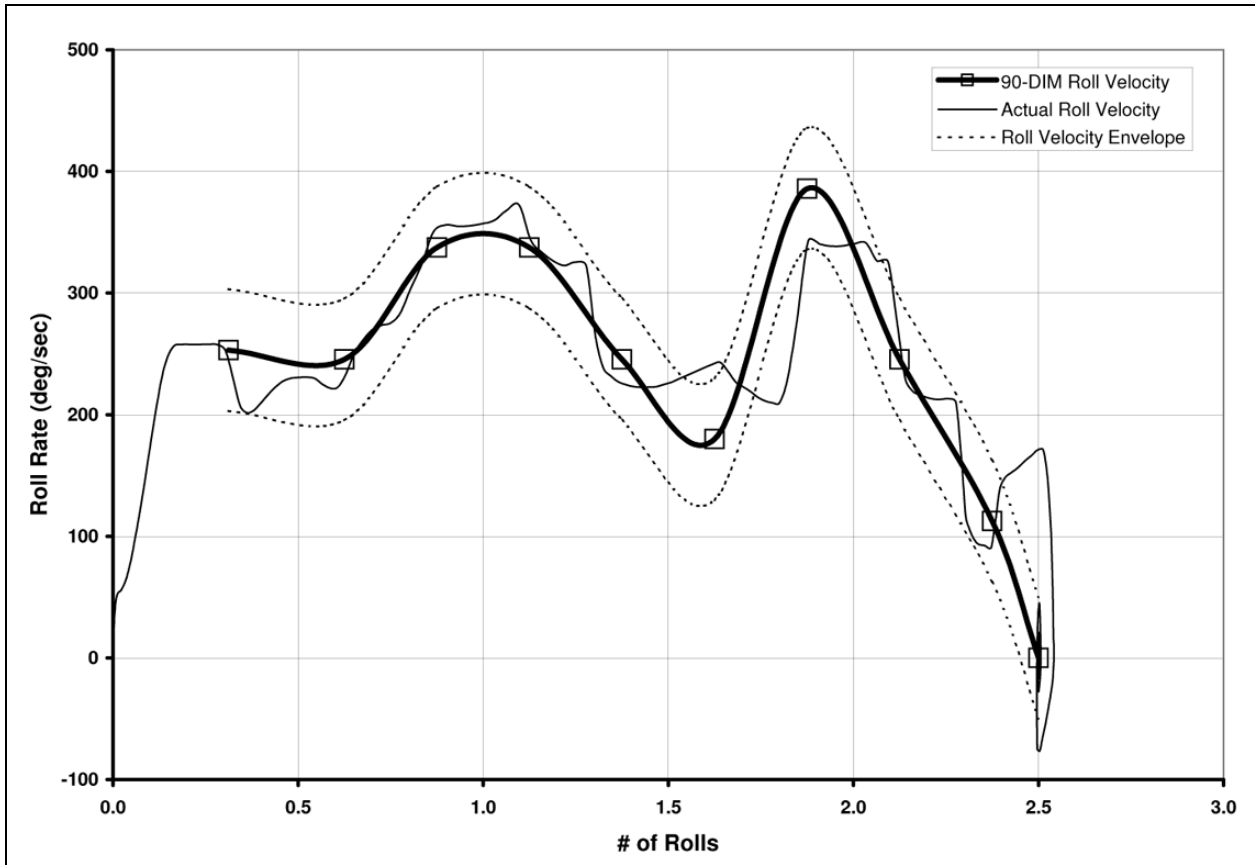


Figure A1 – Case B, Roll Rate v. Number of Rolls

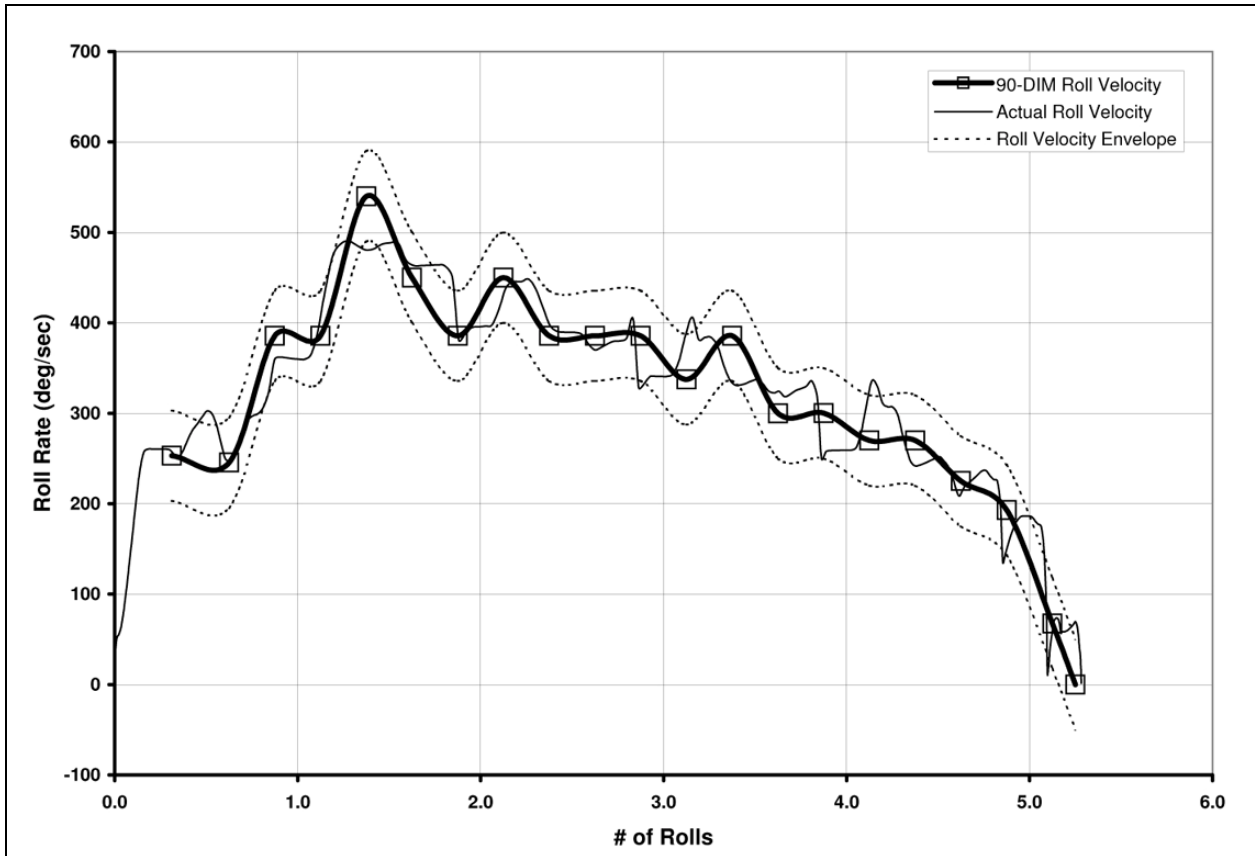


Figure A2 – Case C, Roll Rate v. Number of Rolls

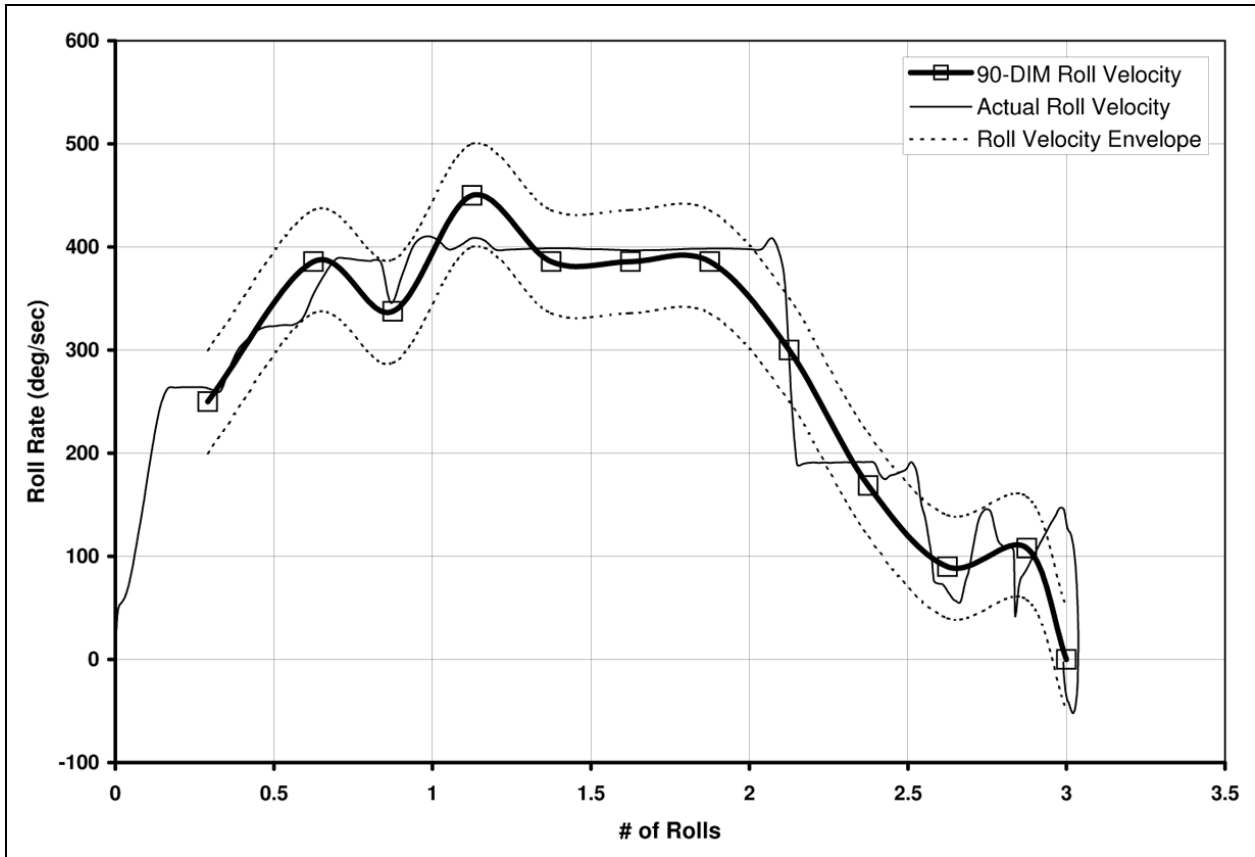


Figure A3 – Case D, Roll Rate v. Number of Rolls

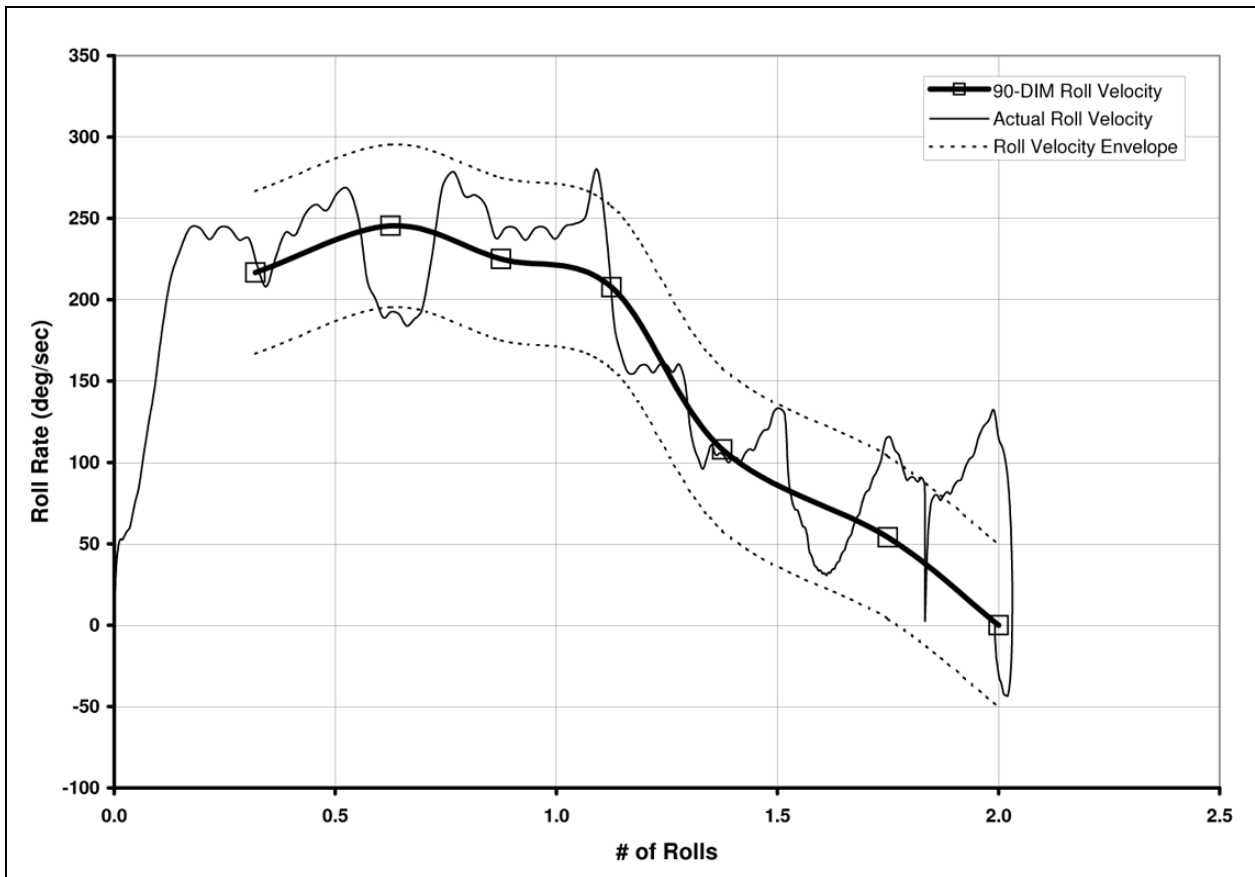


Figure A4 – Case E, Roll Rate v. Number of Rolls

APPENDIX B – TRIP PHASE MODEL DEVELOPMENT

The model depicted in Figure 28 has the following equations of motion:

$$ma_y = F_T \quad (B-1)$$

$$ma_z = N - mg \quad (B-2)$$

$$I_{xx}\alpha_r = F_T \cdot \delta \cdot c(\lambda - \theta_r) - N \cdot \delta \cdot s(\lambda - \theta_r) \quad (B-3)$$

In Equations (B-1) through (B-3), a_y is the CoM ground plane acceleration, a_z is the CoM vertical acceleration, α_r is the roll axis angular acceleration of the vehicle, m is the vehicle mass, I_{xx} is the vehicle roll moment of inertia, F_T is the time dependent tripping force, N is the normal load at the leading wheels, θ_r is the vehicle roll angle and δ is a geometric parameter defined as follows:

$$\delta = \sqrt{h^2 + \left(\frac{T}{2}\right)^2} \quad (B-4)$$

Thus, δ is the distance from the vehicle CoM to the point of the trip force application. The angle λ in Equation (B-3) is defined as follows:

$$\lambda = \tan^{-1}\left(\frac{T}{2h}\right) \quad (B-5)$$

During the trip phase, the leading side wheels remain in contact with the ground, and thus, Equations (B-1) through (B-3) are supplemented with the following geometric constraint equation:

$$z = \delta \cdot c(\lambda - \theta_r) \quad (B-6)$$

Differentiation of Equation (B-6) twice with respect to time yields Equations (B-7) and (B-8), which give the vertical velocity and vertical acceleration of the CoM, respectively. The symbol ω_r represents the roll velocity.

$$v_z = \delta \cdot \omega_r \cdot s(\lambda - \theta_r) \quad (B-7)$$

$$a_z = \delta \cdot \alpha_r \cdot s(\lambda - \theta_r) - \delta \cdot \omega_r^2 \cdot c(\lambda - \theta_r) \quad (B-8)$$

Substitution of Equation (B-8) into Equation (B-2) yields Equation (B-9), which describes the leading side normal load as a function of the vehicle weight, roll angle, roll velocity, and roll acceleration.

$$N = mg + m\delta \cdot \alpha_r \cdot s(\lambda - \theta_r) - m\delta \cdot \omega_r^2 \cdot c(\lambda - \theta_r) \quad (B-9)$$

Substitution of Equation (B-9) into Equation (B-3) leads to Equation (B-10), a nonlinear, second-order ordinary differential equation describing the angular motion of the rigid vehicle.

$$\alpha_r = \frac{\left(F_T \delta \cdot c(\lambda - \theta_r) - mg \delta \cdot s(\lambda - \theta_r) \right) - \left(m\delta^2 \omega_r^2 s(\lambda - \theta_r) c(\lambda - \theta_r) \right)}{I_{xx} + m\delta^2 s^2(\lambda - \theta_r)} \quad (B-10)$$

Equations (B-11) and (B-12) represent an Euler's method numerical integration scheme for Equation (B-10).

$$\theta_{r,t} = \omega_{r,t-\Delta t} \Delta t + \theta_{r,t-\Delta t} \quad (B-11)$$

$$\Delta \omega_{r,(t-\Delta t) \rightarrow (t)} = \frac{\left(F_T \cdot \delta \cdot c(\lambda - \theta_{r,t}) - mg \cdot \delta \cdot s(\lambda - \theta_{r,t}) + m \cdot \delta^2 \cdot s(\lambda - \theta_{r,t}) \cdot c(\lambda - \theta_{r,t}) \cdot \omega_{r,t-\Delta t}^2 \right)}{I_{xx} + m \cdot \delta^2 \cdot s^2(\lambda - \theta_{r,t})} \cdot \Delta t \quad (B-12)$$

To obtain a solution relevant to a particular case, the trip phase duration is prescribed and the magnitude of the tripping force is iteratively changed until the normal load on the leading tires goes to zero at the prescribed trip duration. The following initial conditions are used for this analysis:

$$\theta_0 = 0 \quad (B-13)$$

$$\omega_0 = 0 \quad (B-14)$$

APPENDIX C – ROOF-TO-GROUND IMPACT MODEL

This appendix develops equations for the planar roof-to-ground impact shown in Figure 35. The development of these largely follows the development of the planar impact equations presented by Reference 17 for a vehicle-to-vehicle impact, with the exception that a gravity impulse is included. The vehicle in this figure is depicted with translational velocity both along and into the ground plane and with a positive roll velocity. Given that this is a planar model, vehicle pitch and yaw motions are neglected. The impact force transfer is assumed to occur instantaneously and at a single point.

The principle of impulse and momentum dictates the following equalities:

$$mv_{zf} - mv_{zi} = P_z - P_g \quad (C-1)$$

$$mv_{yf} - mv_{yi} = P_y \quad (C-2)$$

$$mk_r^2(\omega_{r,f} - \omega_{r,i}) = P_y \cdot d \cdot s\phi - P_z \cdot d \cdot c\phi \quad (C-3)$$

In Equations (C-1) through (C-3), k_r is the vehicle's radius of gyration for the roll axis, d is the distance between the vehicle CoM and the point at which the impact force is applied to the vehicle roof (Point C), ϕ is the angle between the orientation of the ground plane and the line connecting the CoM to Point C, P_z and P_y are the normal and tangential impulse components that result from the impact and P_g is the gravity impulse. Translational velocity components are denoted with the letter v and final and initial velocities are denoted with the subscripts f and i .

The gravity impulse can be rewritten with the following equations:

$$P_g = mg \cdot \Delta t_i \quad (C-4)$$

In Equation (C-4), g is the gravitational constant and Δt_i is the impact duration.

The following constraint equations govern the impact energy loss along the normal and tangential directions:

$$e = -\frac{v_{zf} - d \cdot c\phi \cdot \omega_{r,f}}{v_{zi} - d \cdot c\phi \cdot \omega_{r,i}} \quad (C-5)$$

$$\mu = \frac{P_t}{P_n} \quad (C-6)$$

In Equations (C-5) and (C-6), e is the coefficient of restitution for the impact and μ is the impulse ratio, which defines the magnitude of the tangential impulse relative to the magnitude of the normal impulse.

With Equations (C-1) through (C-6), the following set of equations can be obtained that describe the CoM velocity changes that the vehicle experiences during the impact depicted in Figure 35:

$$\Delta V_z = - \left[\begin{array}{l} (1+e) \cdot v_{zc,i} \cdot \left\{ \frac{k_r^2}{k_r^2 + d^2(c^2\phi - \mu \cdot s\phi \cdot c\phi)} \right\} + \\ g \cdot \Delta t_i \cdot \left\{ \frac{d^2(c^2\phi - \mu \cdot s\phi \cdot c\phi)}{k_r^2 + d^2(c^2\phi - \mu \cdot s\phi \cdot c\phi)} \right\} \end{array} \right] \quad (C-7)$$

$$\Delta V_y = \mu \cdot \Delta V_z \quad (C-8)$$

$$\Delta \omega_r = -(\Delta V_z + g \cdot \Delta t_i) \cdot \frac{d \cdot (c\phi - \mu \cdot s\phi)}{k_r^2} \quad (C-9)$$

In Equation (C-7), $v_{zc,i}$ is the vertical velocity at Point C immediately preceding the impact, defined as follows:

$$(C-10) \quad 36$$

$$v_{zc,i} = v_{zi} - d\omega_{r,i} \cdot c\phi$$

The energy loss during the impact depicted in Figure 35 can be written as follows:

$$E_d = \frac{1}{2} m \left(v_{zi}^2 - v_{zf}^2 + v_{yi}^2 - v_{yf}^2 + k_r^2 \left\{ \omega_{r,i}^2 - \omega_{r,f}^2 \right\} \right) \quad (C-11)$$

Again, since we are considering a planar impact model, energy losses or gains associated with changes in pitch and yaw velocity are neglected in this equation. Equation (C-11) can be rewritten in terms of the CoM vertical velocity change, the roll velocity change, and the initial velocity conditions by considering using the following relationships:

$$v_{zi}^2 - v_{zf}^2 = -\Delta V_z^2 - 2v_{zi}\Delta V_z \quad (C-12)$$

$$v_{yi}^2 - v_{yf}^2 = -2\mu v_{gi}\Delta V_z - \mu^2 \Delta V_z^2 \quad (C-13)$$

$$\omega_{r,i}^2 - \omega_{r,f}^2 = -2\omega_{r,i}\Delta\omega_{roll} - \Delta\omega_{roll}^2 \quad (C-14)$$

Substitution of these expressions into Equation (C-11) results in the following equation:

$$E_d = -\frac{1}{2} \cdot m \cdot \left[\begin{array}{l} \Delta V_z^2 (1 + \mu^2) + \\ 2\Delta V_z (v_{zi} + \mu v_{gi}) + \\ k_r^2 \Delta \omega_r (2\omega_{r,i} + \Delta \omega_r) \end{array} \right] \quad (C-15)$$

The energy loss quantified by Equation (C-15) includes the energy loss due to vehicle deformation, the energy loss due to sliding and snagging between the vehicle structure and the ground, and the energy dissipated by the ground. Assuming that the ground absorbs negligible energy and that the ground plane impulse does not deform the vehicle structure, the portion of the total energy loss of Equation (C-14) absorbed through vehicle deformation can be estimated by calculating the work done by the vertical direction impulse during the impact.

As stated in Reference 17, the work done by an impulse can be obtained with the following equation:

$$W_P = P \cdot \frac{v_i + v_f}{2} \quad (C-16)$$

In Equation (C-16), P is the impulse and v_i and v_f are the initial and final velocities at the point of force application. This equation states that the work done by an impulse is equal to the product of the impulse and the average velocity along the line of action of the impulse. For the vertical impulse transferred during the impact depicted by Figure 35, Equation (C-16) takes the following form:

$$W_{P,z} = -E_{d,z} = P_z \cdot \frac{v_{zc,i} + v_{zc,f}}{2} \quad (\text{C-17})$$

Substituting Equations (C-1) and (C-10), along with an expression analogous to Equation (C-10) for the final vertical velocity at Point C, yields the following equation:

$$E_{d,z} = -\frac{m}{2} \cdot (1-e) \cdot v_{zc,i} \cdot (\Delta V_z + g\Delta t_i) \quad (\text{C-18})$$

There will certainly be cases when the ground will absorb a substantial quantity of energy and when the ground plane impulse will deform a vehicle's roof structure. In these cases, Equation (C-18) will not accurately characterize the deformation energy for the impact.